POLITECNICO DI MILANO

Facoltà di Ingegneria Industriale

Corso di Laurea Specialistica in
Ingegneria Spaziale

On-comet attitude determination of Rosetta lander Philae through nonlinear optimal system identification

Relatore: Prof. Franco Bernelli Zazzera
Co-relatore: Ing. Francesco topputo

Tesi di Laurea di:
Gianluca M. Caputo 725121

Anno Accademico 2011-2012

Abstract

This thesis concerns the development of an algorithm capable to extrapolate the Sun incidence angles, defined as azimuth α and elevation β, from a power telemetry file obtained during First Science Sequence performed by lander Philae in the ESA Rosetta mission. The objective is the definition of the direction of optimum power production, coupled with the attitude correction rotation needed to point the lander towards it.

Sommario

Questa tesi riguarda lo sviluppo di un algoritmo capace di ricavare gli angoli di incidenza del Sole, definiti come azimuth α ed elevazione β, a partire dal file di telemetria di potenza ottenuto durante la fase di Prima Ricerca Scientifica effettuata da Philae, il lander della missione Rosetta sviluppata dall'ESA. L'obiettivo finale è la definizione della direzione di ottima potenza, e la rotazione di assetto necessaria per puntare il lander verso essa.

Ringraziamenti

Ringrazio il Prof. Bernelli per avermi dato la possibilità di lavorare su un progetto così interessante e il Dott. Topputo per la grande pazienza e i consigli che mi hanno aiutato nel raggiungere i risultati conseguiti. Ringrazio anche il Dott. Pinzan senza i cui dati la fine sarebbe ancora lontana.

Da menzionare Alessandro, Valentina, Fabio, Marco, Giorgio, Vittorio, Francesco, Filippo e tanti altri, che hanno militato assieme a me in questa imperitura avventura della nostra vita, e per tutto l'aiuto che mi hanno dato, anche quando non se ne rendevano conto.

Ringrazio infinitamente i miei genitori per la grande opportunità che mi hanno dato, e senza i quali non sarei chi sono oggi.

Il mio primo e ultimo pensiero va a Cecilia, per la quale non basterebbero mille parole: grazie.

Contents

List of Figures

List of Tables

Determinazione dell'assetto del lander Philae attraverso identificazione non lineare dei parametri del sistema di potenza

La missione Rosetta Sviluppata dall'ente spaziale europeo ESA, questa missione ha come obiettivo quello di investigare il nucleo di una cometa attraverso analisi di tipo chimico, fisico e mineralogico. Rosetta, lanciata nel 2004, ha come meta finale la cometa 67P Churyumov-Gerasimenko con un randez vou alla distanza di circa 3 AU, dopo aver volato vicino agli asteroidi 2867 Steins e 21 Lutetia.

Una volta raggiunta destinazione l'orbiter Rosetta comincerà ad orbitare attorno all'obiettivo, eseguendo un'analisi della miglior traiettoria e zona di atterraggio per il lander Philae.

Durante il volo il lander è alimentato dal sistema di potenza dell'orbiter, ma una volta sganciato, ovvero fin dall'inizio della traiettoria di discesa, dovrà provvedere autonomamente al proprio sostentamento. Philae è alimentato da una batteria Primaria (1000 Wh) e da una Secondaria (130 Wh), assieme ad un sistema di pannelli solari.

Le batterie assicurano la sopravvivenza fino alla fine della fase operativa di Prima Ricerca Scientifica (FSS). L'uso dei pannelli solari serve ad estendere la vita del lander attraverso la modalità operativa di Ricera Scientifica a Lungo Termine (LTS). Una superficie totale di 2 m^2 di celle solari LILT (Low-Intensity Low-Temperature) è distribuita su 6 pannelli, uno per ognuna delle 6 facce diverse di Philae. Il sistema produrrà una potenza totale fino a 8 W, che verrà incanalata su un bus di 28 V attraverso un sistema di 5 MPPT (Maximum Power Point Tracker). Questi ultimi hanno come obiettivo la ricerca del punto di massima potenza sulle curve IV (Voltaggio-Corrente)

attraverso uno scanning delle stesse ad una frequenza di circa 30-60 Hz.

Telemetria di Potenza Il file di riferimento ha una estensione "*.xls", e presenta i segnali di corrente in uscita dagli MPPT in mA, ordinati come segue: Wall2, Wall3, Wall4, Wall6, Wall1+5. L'ultimo è assegnato a due pannelli, poichè questi sono posizionati su facce opposte del lander e non posso quindi essere illuminati simultaneamente.

Simulatore dei Pannelli Solari Il programma PSAS (Philae Solar Array Simulator) è un pacchetto di programmi sviluppato all'interno del Politecninco di Milano, e permette di definire le curve IV dei pannelli solari, che fungeranno da input per il simulatore hardware del sistema di potenza. Esso inoltre calcola le prestazioni dei pannelli solari attraverso una funzione non lineare degli angoli di incidenza solari, del tempo, della distanza dal Sole, della temperatura e infine della radiazione assorbita totale. PSAS fungerà da base per lo sviluppo dell'algoritmo della tesi, grazie alla capacità di ottenere la corrente in uscita dai pannelli solari a partire da elevazione e azimuth del Sole espressi negli assi corpo di Philae.

Motivazioni e definizione del problema L'interesse principale, oltre a quello di assicurare la sopravvivenza del lander oltre la fase FSS, è quello di massimizzare la produzione di potenza, così da poter riuscire a svolgere un maggior numero possible di esperimenti scientifici nel tempo trascorso sulla cometa.

L'obiettivo della tesi è quello di ottenere gli angoli di incidenza del Sole azimuth ed elevazione, definiti negli assi corpo di Philae nel corso della giornata cometaria, così da poter ricavare l'orientamento capace di massimizzare la produzione di potenza. Dal momento che la corrente in uscita dagli MPPT è una funzione non linerare degli angoli di incidenza del Sole, è necessario trovare la soluzione attraverso un problema inverso: la definizione di un problema di estimazione dei parametri capace di ricavare i valori desiderati a partire dall'osservazione degli stati del sistema dinamico.

Noto il modello che descrive il fenomeno di generazione di potenza sui pannelli solari del lander, l'obiettico è definire un algoritmo capace di ottenere gli angoli di azimuth ed elevazione del Sole nel periodo di tempo descritto dal file di telemetria, questo attraverso una procedura di ottimizzazione per ottenere i parametri che hanno prodotto i segnali di corrente campionati.

Assunzioni E' necessario presentare le assunzioni prese durante lo sviluppo dell'algoritmo in quanto ne influenzano il corretto funzionamento nel caso

non venissero rispettate. Si assume che i pannelli siano illuminati solo dalla luce solare diretta, senza l'influenza di albedo o riflessi di alcun genere. Nessuna formazione di ghiaccio o polvere è prevista sui pannelli solari, che lavorano con l'area totale fornita dai data sheet. La superficie della cometa è considerata piatta, senza valli od ostacoli che possano fare ombra. Per finire, si assume che le telemetrie create tramite un simulatore di MPPT applicato a PSAS, che genera disturbi sui segnali di corrente in uscita simili a quelli forniti da telemetrie ufficiali, siano da considerare attendibili.

Preprocessing I segnali di corrente campionati nella telemetria vanno trattati prima di essere utilizzati nei processi di calcolo degli angoli di incidenza del Sole.

Dopo che la telemetria viene caricata, tramite un'apposita finestra di dialogo, viene definito un valore minimo di corrente, sotto al quale si considera il segnale come rumore di fondo: tutto ciò che è sopra tale valore identifica la potenza prodotta. Successivamente si puliscono i picchi fuori scala tramite la distribuzione di probabilità applicata ai segnali.

La pulizia del segnale può essere effettuata tramite una frequenza di taglio oppure tramite la tecnica dello smoothing. Pur essendo disponibile nell'algoritmo, data la difficoltà nella definizione di una frequenza di taglio, si è preferito come metodo principale quello dello smoothing. Tramite questa tecnica i punti discreti di un segnale sono modificati in modo che i valori individuali che sono superiori a quelli adiacenti vengano diminuiti e viceversa. Questo porta ad un segnale più pulito e meno spigoloso, e l'effetto è quello della diminuzione del rumore bianco. Detta s la sua deviazione standard, essa diminuisce ad ogni passo secondo la regola $(s/sqrt(m))$, dove m è il passo dello smoothing, ovvero i punti presi attorno al valore in considerazione.

Tempo di riferimento e Finestre di Produzione di potenza Poichè i segnali di corrente degli MPPT vengono campionati a tempi diversi, è necessario un tempo di riferimento per riuscire a definire gli angoli di incidenza. Per fare ciò è stato preso come riferimento il vettore del primo MPPT campionato ad ogni ciclo, mentre gli altri MPPT sono linearmente interpolati rispetto ad esso. Il primo valore del vettore tempo è invece quello dell'ultimo MPPT campionato al primo ciclo. In questa maniera si assicura la rimanenza all'interno del lasso di tempo presentato dal file di telemetria, così da assicurare l'utilizzo delle sole informazioni disponibili.

Le finetre di potenza sono dei lassi di tempo utili per sapere quando c'è effettiva produzione di corrente, ed iniziano o finiscono quando un pannello solare comincia o finisce di produrre potenza. Il vantaggio è che ogni finestra

è caratterizzata da una combinazione ben definita di pannelli illuminati, dove gli altri sono considerati spenti.

Soluzione di Primo tentativo Capace di rappresentare con accettabile approssimazione l'andamento reale degli angoli di incidenza del Sole, serve per evitare di trovare soluzioni di minimo locali e per velocizzare i tempi computazionali. Viene calcolata tramite una soluzione lineare, e tutti gli effetti non lineari sono per approssimazione inclusi dentro l'efficienza totale.

La potenza dei pannelli illuminati viene calcolata secondo la formula

$$\mathbf{P} = 28\,\mathbf{I} = \mathbf{s} \cdot \mathbf{N}\; Diag(\mathbf{A})\; \eta,$$

dove 28 è il voltaggio del Bus, $\mathbf{I}$ il vettore delle relative correnti, $Diag(\mathbf{A})$ la matrice diagonale delle corrispondenti aree dei pannelli, $\mathbf{N}$ i relativi versori normali, ed infine η l'efficienza totale.

Invertendola si ottiene

$$\mathbf{S}_\eta = S\,\eta\,\mathbf{s} = (\mathbf{N}\; Diag(\mathbf{A}))^{-1}\, 28\,\mathbf{I}$$

.

Infine, cercando il versore di Direzione del Sole, si può togliere la dipendenza dalla efficienza tramite

$$\mathbf{s} = \frac{\mathbf{S}_\eta}{|\mathbf{S}_\eta|}$$

dove l'unica approssimazione presa è stata l'assegnazione delle non linearità al coefficiente dell'efficienza. Gli angoli di incidenza del Sole sono ricavati dalle componenti del versore direzione Sole secondo il seguente metodo:

$$\alpha = \begin{cases} \arctan\left(\frac{s_x}{z_y}\right) & s_y \geq 0 \\ \arctan\left(\frac{s_x}{z_y}\right) + 180^\circ & s_y < 0 \end{cases}$$

$$\beta = arcsin(s_z).$$

Perchè $\mathbf{N}$ sia invertibile deve essere quadrata, richiedendo che i pannelli accesi siano 3 o più, di cui almeno uno sia il pannello 6. Nel caso fossero più di 3, le eventuali combinazioni di pannelli accesi forniscono un numero maggiore di soluzioni, che mediate tra loro dovrebbero diminuire le incertezze dovute alle approsimazioni prese.

Problema di Estimazione dei Parametri applicato alla ricerca della angoli di incidenza del Sole I parametri da identificare sono gli angoli di incidenza del Sole, e per ogni ciclo di campionamento j-esimo di correnti esiste una coppia di angoli, azimuth ed elevazione, che viene inserita nel vettore dei parametri

$$\mathbf{x} = \{\alpha_j, \ldots, \alpha_n, \beta_j, \ldots, \beta_n\}.$$

Il vincolo non lineare a cui la coppia di angoli deve sottostare è definito dal modulo del versore direzione del Sole, che deve essere unitario

$$g(\mathbf{x}) = (cos(\beta) \cdot sin(\alpha))^2 + (cos(\beta) \cdot cos(\alpha))^2 + (sin(\beta))^2 - 1 = 0.$$

I vincoli riguardanti le condizioni al contorno sono definiti tramite la combinazione di pannelli accesi, fornendo in questa maniera un arco di azimuth ed elevazione in cui la soluzione deve necessariamente cadere.

Volendo diminuire il tempo computazionale necessario per trovare la soluzione si cercano i parametri di un numero inferiore di tempi campionati rispetto al totale, mentre l'indice di prestazione è calcolato tenendo conto di tutti i campioni, dove quelli non computati sono ottenuti tramite interpolazione linerare. L'indice di prestazione è quindi formulato nella seguente maniera

$$F(\mathbf{x}) = \sum_i (\bar{\mathbf{Y}}_i - \widehat{\mathbf{Y}}_i)^T \cdot (\bar{\mathbf{Y}}_i - \widehat{\mathbf{Y}}_i),$$

dove $\bar{\mathbf{Y}}_i$ è la corrente computata per interpolazione mentre $\widehat{\mathbf{Y}}_i$ è la corrente da telemetria, entrambe facenti riferimento al pannello i-esimo.

Da ricordare che le correnti dei pannelli sono funzioni di elevazione ed azimuth anche attraverso la temperatura dei pannelli, che dipendono dall'incidenza della radiazione solare, e sono calcolabili tramite modello fornito. Si può quindi scrivere il problema di estimazione dei parametri nella seguente maniera

$$\min_{LB \leq \mathbf{x} \leq UB} \quad F(\mathbf{x}) \quad subject\ to \quad g(\mathbf{x}).$$

Rotazione d'assetto Per massimizzare la potenza prodotta nell'arco della giornata cometaria è necessario orientare il lander verso una direzione definita a seconda del tipo di scenario affrontato: durante la classica giornata cometaria, in cui è presente anche un periodo di tempo associabile alla notte, è definita dalla elevazione massima; da elevazione minima quando avviene l'Hovering, ovvero il Sole è sempre visibile; dall'azimuth posto a metà tra alba e tramonto quando si ha intersezione del Sole con lo zenith del lander. Nel caso di notte perpetua la definizione di tale rotazione è inutile.

Graphical User Interface Assieme all'algoritmo è fornita una interfaccia grafica capace di caricare e mostrare le soluzioni del problema, permettendo all'utente di evitare una diretta interazione con il codice.

Risultati Per avere un'idea sulla corretezza dei risultati dell'algoritmo sono state utilizzate delle telemetrie costruite a partire da storie temporali di azimuth ed elevazione già note. Nel caso del comune giorno cometario l'algoritmo ha dato prova di riuscire a ottenere dei buoni risultati, sia come andamento della soluzione finale, capace di seguire bene gli andamenti esatti, sia come definizione della direzione di produzione di potenza ottima, risultando in un incremento sensibile della energia accumulata. Nello scenario di Hovering la soluzione presenta le stesse accuratezze riscontrate nel caso del comune giorno cometario. Nel caso in cui la scelta attuata dall'algoritmo riguardo la direzione di produzione di potenza ottima fosse evidentemente sbagliata, a causa di eventuale permanenza di errori nel segnale agli estremi del periodo di campionamento, la generale qualità del segnale permette in ogni caso di poter ricavare autonomamente i valori necessari.

L'unica situazione in cui la soluzione tende a scostarsi dagli andamenti esatti è quella in cui il Sole passa per lo zenith del lander, esasperando tutti i disturbi che si tendono ad avere quando la luce ha poca incidenza rispetto ai pannelli. In questo caso vengono fornite a supporto dell'utente una serie di informazioni aggiuntive rispetto alla soluzione finale, come ad esempio la soluzione di primo tentativo o la definizione delle condizioni al contorno dei segnali, che forniscono i mezzi necessari per ricavare i valori necessari tramite una loro analisi critica.

Infine la telemetria fornita per testare l'algoritmo, ottenuta tramite un simulatore hardware, e di cui non è stata fornita la soluzione esatta, ha permesso di verificare l'ottenimento di valori soddisfacenti anche senza avere alcun riferimento.

Conclusioni L'algoritmo ha ampiamente provveduto a dimostrare di essere capace di fornire tutti gli strumenti necessari per riuscire ad ottenere le storie temporali degli angoli di incidenza del Sole, anche quando la soluzione finale non fosse perfettamente in linea con i valori esatti. Questo permette di ottenere incrementi nella potenza prodotta dai panelli solari, con guadagni anche di notevole entità per la maggior parte dei casi.

Chapter 1

Introduction

In this chapter the purposes and the scientific targets of the Rosetta Mission will be shown, including a brief presentation of mission, the asteroids visited along the journey and the target comet 67P/Churyumov-Gerasimenko. Being composed of the Rosetta space probe and the lander Philae, particular attention is given to the second, which is the subject of this thesis.

1.1 The Rosetta Mission

The Rosetta mission has been developed by the European Space Agency (ESA) with the objective to investigate a comet's nucleus in detail thorough chemical, physical, and mineralogical analysis that will be radioed to Earth. The purpose is a better comprehension of the origin of the comets, where, being their composition unchanged through the eras, it may lead to a better understanding of the solar system at its origins [1].

Comets are irregularly shaped chunks of dust and ice, usually on highly elliptical orbits. It is possible to find comets in the largest reservoir present in the Oort Cloud, surrounding the Sun at 100.000 Astronomical Units (AU), or in the the second and significantly smaller present beyond Neptune at 50 AU, the so-called Trans-Neptunian Objects (TNO's), where astronomers found several planet-like objects, residing in the Kuiper-Edgeworth belt. In this group are present Pluto, its moon Charon, and Eris, the dwarf planet that had been discovered in 2003: these are called "'Plutonides"' due to the diameters that not match the classical image of a comet. The asteroid belt located between Mars and Jupiter is formed mainly by irregularly shaped rocks made of stone and metal elements, whilee instead the TNOs are formed by frozen light elements like water ice, carbon dioxide, methane and ammonia.

When disturbed in their orbit in the Oort Cloud, due to the tug of a near star or to galactic tidal forces, some comets got thrown in the direction of

the inner solar system: most of them need centuries or millenia to perform one orbit around the sun. Transneptunian objects complete their orbit in significantly less time. As a comet gets near to the Sun, the star warmth begin to sublimate the icy components of the comet's surface. The gas jets escaping from the nucleus tears dust particles of the comet that are lost in space, which, together with the gas molecules, reflect the sunlight. This way is formed the Coma, the classical tail of a comet, named this way from the Greek word for hair. The escaping dust particles are pushed from the solar radiation and the tail formed by them can be as long as several hundred million kilometers. The gas molecules ionized by the ultraviolet radiation of the sun form instead smaller plasma tail [1].

The comet 67P Churyumov-Gerasimenko Named after the two astronomers, Klim Churyumov and Svetalana Gerasimenko, who discovered it, this comet has been chosen as target of the mission. The orbit has greatly changed in the last century: at the beginning, earlier than the year 1840, the comets perihelion was at a distance from the sun of 4 Astronomical Units (AU), but varied after a close flight near Jupiter, due to the gravitation tug of the planet. In a century the perihelion decreased to 2.77 AU, and, after a new encounter with Jupiter, reached the present value of 1.29 AU. Consequently the aphelion reached the value of 5.74 AU, with an orbital period of 6.75 years and an inclination to the ecliptic of 7 degrees. Gathered informations from the last decades present a comet whose 3-5 km tail sprays 60 kilograms of dust per second, a rotational period of about twelve hours and a first 3D model of the nucleus [1]. In fig. 1.1 it is possible to see a 3D reconstruction of the target comet made thanks to a telescope Hubble analysis.

The Rosetta mission ESA started the mission in 1993, which represents one of the agency cornerstone missions in "'Horizon 2000"' program, with the goal to enhance our understanding of the formation and evolution of the Solar System as well as the origin of life, by investigating a comet remotely. The mission name is taken from the Egyptian town of Rashid, or Rosetta, where archaeologists found in 1979 a stone incised with scripts three different ancient languages. Together with an obelisk from the town of Philae archaeologists were able to decipher the completely enigmatic hieroglyphs. The hope is to do the same with the data gathered from the 67P comet [1]. The main tasks are:

- global characterization of the comet's nucleus and surface topography
- characterization of both the chemical and mineralogical composition, and the isotopic relations

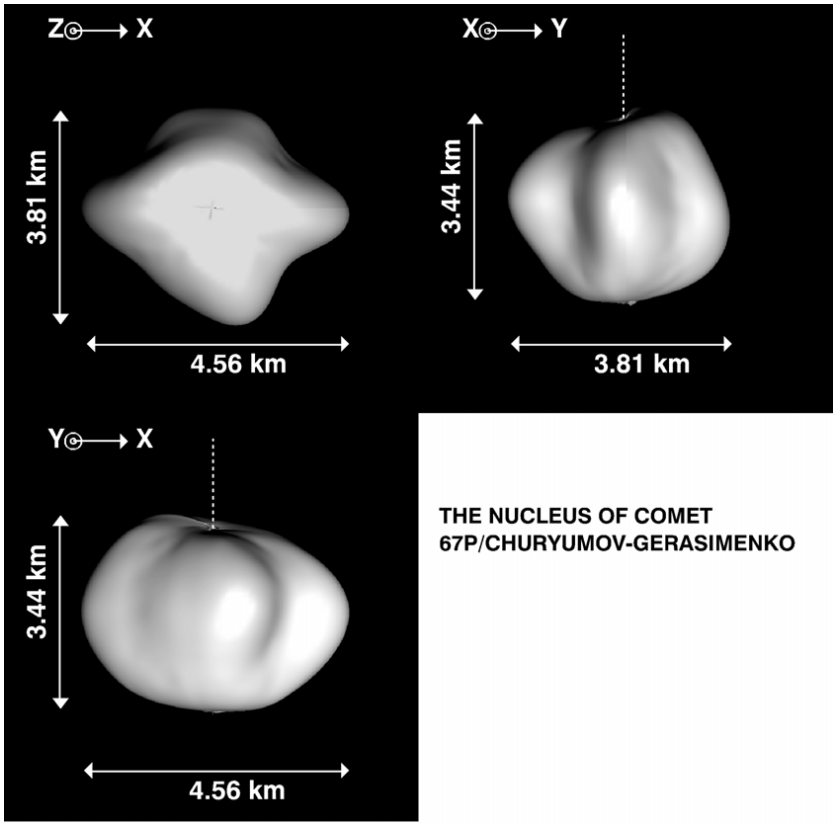

Figure 1.1: 3D reconstruction of the comet 67P [2]

- derivation of physical properties of the comet's nucleus, like structure and thermal, electrical and magnetic properties, and monitoring of cometary activity while approaching the sun.

The spacecraft was launched 2 March 2004 on an Ariane 5 rocket from Kourou in French Guyana, with a mission flight of 10 years with a rendezvous with 67P Churyumov-Gerasimenko in 2014.

From the commissioning the Rosetta probe had several swing-byes manoeuvres at Earth and Mars in order to reach the comet 67P, and, as programmed, successfully flew-by two asteroids along its flight: asteroid 2867 Steins, on 5 September 2008, and asteroid 21 Lutetia, on 10 July 2010. These additional objectives have been used to give more data and photos on other important small Solar System bodies [1].

Following the fly-by of Lutetia the mission entered a four-year long hibernation mode, waiting to reach the target asteroid. In January 2014 the spacecraft will be awaken for mission control. The approach will happen in the period January-May 2014 at a distance of 3 AU circa from the Sun: as

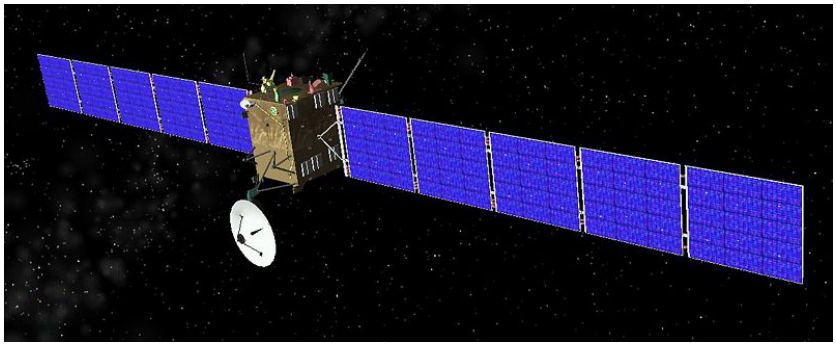

Figure 1.2: Rosetta Probe with solar panels unfolded [ESA]

the space prob gets closer, around August 2014, it will start the mapping and the characterization of Churyumov-Gerasimenko. Once reached it will start to orbit around the target and start an analysis to define the best trajectory and landing zone for the Philae deployment.

After the separation the Rosetta space probe will escort the comet around the Sun in a period that goes from November 2014 to December 2015, keeping track of the analysis of the comet properties along its orbit around the Sun and working as communication bridge between mission control and the lander Philae.

The Rosetta design is based on a box-type central structure, 2.8 m x 2.1 m x 2.0 m, on which all subsystems and payload equipment are mounted. The spacecraft electrical system run thanks to the 440 Watt provided by the two solar panels of a total area of 64 square meters (in fig. 1.2), that once unfolded stretch out to 14 meters in length, giving a total length of 32 meters from tip to tip. The lander Philae is attached to the spacecraft side opposite to the one carrying the 2.2 meters wide high gain antenna. The combined launch weight of Orbiter and lander is 2.9 tons, of which approximately 1.5 are fuel.

The scientific instruments on board of the Rosetta [4]orbiter are:

- **ALICE** An ultraviolet imaging spectrograph (Alan Stern, SRI, Boulder (USA))
- **OSIRIS** Optical, Spectroscopic, and Infrared Remote Imaging System (Horst-Uwe Keller, MPS, Lindau (D))
- **VIRTIS** Visible and Infrared Thermal Imaging Spectrometer (Angioletta Coradini, IAS-CNR, Rome, (I))
- **Miro** Microwave Instrument for the Rosetta Orbiter (Sam Gulkis, JPL, Pasadena, (USA))

- **CONSERT** Comet Nucleus Sounding Experiment by Radiowave Transmission (Wlodek Kofman, LPG, CNRS/UJF, Grenoble (F))
- **ROSINA** Rosetta Orbiter Spectrometer for Ion and Neutral Analysis (Hans Balsiger, Universit¨at Bern (CH)
- **MIDAS** Micro-Imaging Dust Analysis System (Willi Riedler, IWF, Graz, (A))
- **COSIMA** Cometary Secondary Ion Mass Analyzer (Martin Hilchenbach (formerly Jochen Kissel), MPS, Lindau (D))
- **GIADA** Grain Impact Analyzer and Dust Accumulator (Luigi Colangelo, INAF, Naples (I))
- **RPC** Rosetta Plasma Consortium (Anders Eriksson (formerly Rolf Bostrom), IRF Uppsala IRF Uppsala, (S), Jim Burch, SRI, San Antonio, (USA), Karl-Heinz Glassmeier, IGEP, Braunschweig, (D), Rickard Lundin, IRF, Kiruna (S), Jean-Gabriele Trotignon, LPCE/CNRS, Orleans (F), Chris Carr, Imperial College, London (ENG))
- **RSI** Radio Science Investigation (Martin Patzold, Universitat Koln (D))

1.2 The Lander Philae

The lander Philae will investigate the comet 67P Churyumov-Gerasimenko in-situ, while the space probe Rosetta will operate from orbit. The Lander system has been provided by an international consortium (Germany (lead), France, Italy, Hungary, Finland, UK, Ireland and Austria) and supports a scientific payload of 10 instruments [5]. It is operated by the Lander Control Center (LCC) at DLR, Cologne, and the Science Operation and Navigation Center (SONC) at CNES, Toulouse, via the European Spacecraft Operations Center (ESOC) in Darmstadt. Since the launch the lander has been operational during commissioning, by performing several checkouts as well as some activities for calibration and failure investigation. The location of Philae in the Rosetta configuration is visible in fig. 1.3.

All the manoeuvres during flight are performed by Rosetta, while Philae is prepared to the descent and on-comet operations. The lander entered in the hibernation phase together with the space prob pending to reach the target comet. However separation, descent and landing strategy are not yet outlined as there's the necessity to characterize first the comet nucleus from

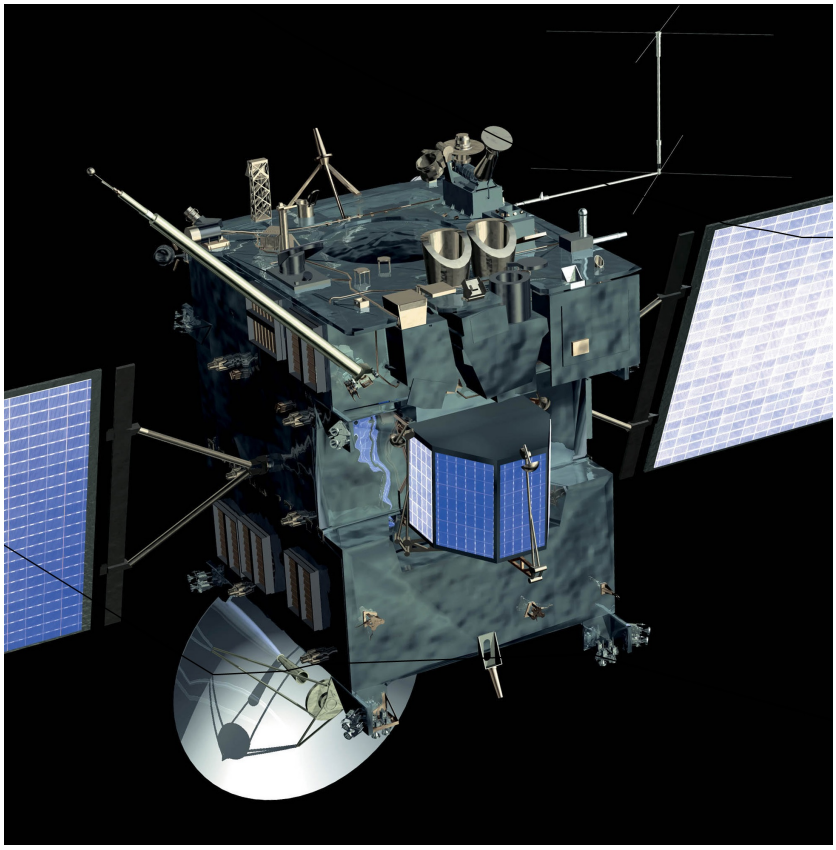

Figure 1.3: Philae configuration on Rosetta Space Probe [3]

orbit, where shape, state of rotation, gravitational field as well as gas and dust environment are relevant key parameters.

The deployed configuration of the Lander is visible in the schematic shown in fig. 1.4. The lander is designed to detach itself from the main spacecraft and fall towards the comet along a ballistic trajectory. To reduce the chance of bouncing during initial impact the legs are designed to damp during the landing, and to avoid possible detachment from the comet surface it will harpoon itself to it. Eventually is possible to activate a motor on the Lid to obtain a tighter anchoring to the comet nucleus.

The lander main operative phases are Separation, Descent, and Landing (SDL), First Science Sequence (FSS) and Long Term Science (LTS). The first two phases last for 5 days after the separation from Rosetta space prob and the power demand is satisfied by the primary battery. The LTS instead will last depending on the success of the SAS to produce power [6]. The total mass is about 100 kg, and most of the surface is covered with solar cells, with the objective of extending LTS by providing additional power to the

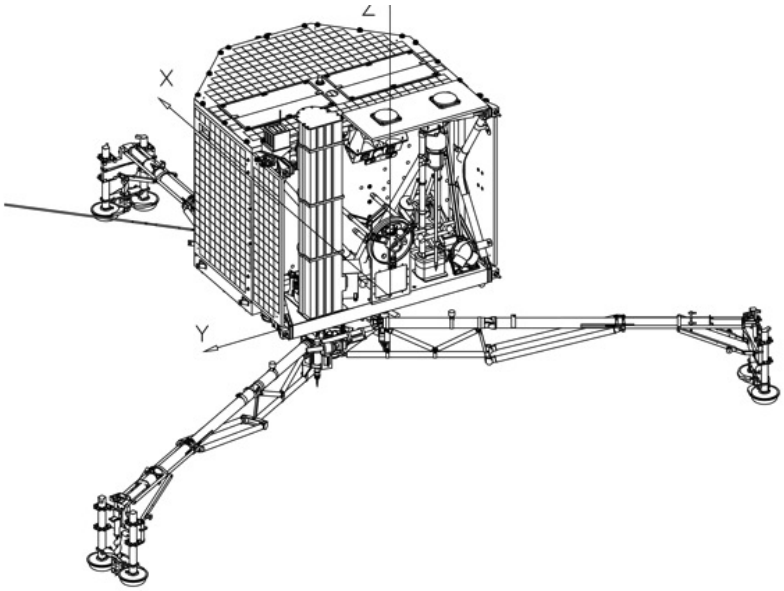

Figure 1.4: Philae configuration after deployment

PSS (Power SubSystem) to charge the secondary battery [7].

The scientific objectives of the Lander are the determination of the composition of cometary surface matter, including the possible presence of organic materials, as well as the investigation of the structure and physical, chemical and mineralogical properties of a comet's surface including the local depth structure (stratigraphy) and global internal structure of a comets nucleus. Communication with Earth of all the data and the telemetry will be through the high gain antenna on Rosetta space probe, which will function as communication bridge . The Rosetta lander scientific instruments are:

- **APX** Alpha Proton X-ray Spectrometer (G. Klingelhofer/R.Rieder; University of Mainz/ Max Planck Inst. (D))
- **COSAC** The COmetary SAmpling and Composition (F. Goesmann, H. Rosenbauer; MPS, Max Planck Inst. (D))
- **Ptolemy** Evolved Gas Analyzer (I.Wright, C.Pillinger, J.Zarnecki; Open University (UK))
- **CIVA** Comet Nucleus Infrared and Visible Analyzer (J.P.Bibring; IAS (F))
- **ROLIS** Rosetta Lander Imaging System (S.Mottola; DLR (D))

- **CONSERT** COmet Nucleus Sounding Experiment by Radiowave Transmission (W.Kofman; LPG (F))
- **MUPUS** MUlti-PUrpose Sensors for Surface and Sub-Surface Science (T.Spohn; University of Munster (D))
- **ROMAP** Rosetta Lander Magnetometer and Plasma Monitor (U.Auster, I.Apathy; Max Planck I. extraterr. Physics, TU Braunschweig(D)/ KFKI (H))
- **SESAME** Surface Electric Sounding and Acoustic Monitoring Experiment (K.Seidensticker, D.Mohlmann, W.Schmidt, I.Apathy; DLR (D)/ FMI (SF)/ KFKI (H))
- **SD2** The sampling, drilling and distribution subsystem (A.Ercoli-Finzi; Politecnico di Milano (I))

1.3 Philae Power SubSystem

The Power SubSystem (PSS) is the system demanded to manage the power generation, control and distribution on the lander. During the cruise phase, when Philae is attached to the Orbiter, all the systems are powered via ESS (Electrical Support System) by the Rosetta power system. Remarkable is that the Rosetta mission is the first deep space mission that will go beyond the main asteroid belt relying only on solar cells for power generation [8].

As Philae is detached, power provision is given by a Battery unit, consisting of a Primary and Secondary unit, and the Solar Array (SA) Generator. The main source of power is represented by the lander Primary Battery, with capacity of 1200 Wh (1000 Wh at comet arrival) capable of feeding the lander up to 5 days to assure the minimum scientific research required by the mission profile, with a support of a Secondary Battery, initial and on comet capacity of 150 Wh and 130 Wh respectively. The Sbatt is rechargeable through Solar Arrays. This configuration is adopted to make possible the Long Term Science (LTS), maximizing the scientific return of the mission by extending the operational life of Philae: as the comet approaches the perihelion of the orbit the solar radiation increases. Power distribution is basically performed via the Lander Primary Bus (non-stabilized, +28 V baseline) [8].

During the comet in-situ investigations there is power production thanks to the 2 m^2 Solar Arrays which will produce about 8 W . This result is achieved thanks to new Low-Intensity Low-Temperature (LILT) solar cells capable to generate energy in the very tough environment in which Rosetta and Philae will have to survive and work. The solar arrays are constituted

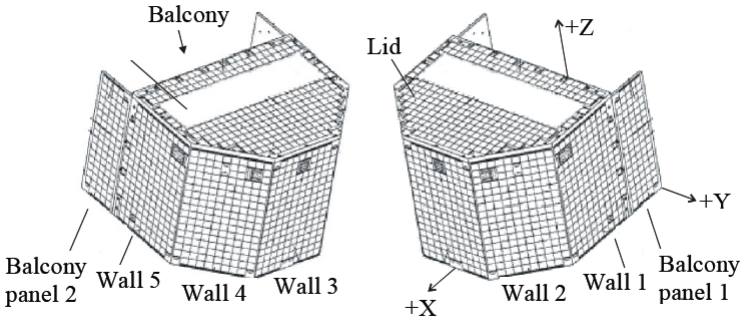

Figure 1.5: Phiale solar array distribution [8]

by 6 panels placed on six different faces not covering every direction, leaving space for scientific payload on one side. The total number of silicon solar cells is 1224 with dimension of 32.4 mm x 33.7 mm, 200 μm thick. In fig. 1.5 is possible to see panels distribution on the lander surface.

The architecture chosen for the electrical system is the Maximum Power Point Tracker system: it places Maximum Power Point Trackers (MPPT) between the solar panels and the loads. Solar cells have complex relationship between solar irradiation, temperature and total resistance that produces a non-linear output efficiency, know as the I-V curve: the use of the MPPT is to obtain the maximum power out of a solar panel by sampling the output of the cells and applying the proper resistance.

While the MPPT conversion efficiency from the solar cell output to the lander bus is relatively high (around 95% or higher) the major loss derives by the scanning along the I-V curve to reach the maximum power point, where the loss is generally higher, up to 25% (see chapter 1.3.1). The six solar panels are connected to the bus via 5 MPPT, where SA1 and SA5 have in common the same tracker due to the fact that are never exposed to direct Sunlight simultaneously.

1.3.1 PSS and Solar Array Simulator

Rosetta is the first deep space mission that will go beyond the main asteroid belt relying only on solar cells for power generation, and the same is for the lander Philae, where, once the batteries are depleted, must rely on solar radiation to extend operational life. For low power systems, in a low intensity, low temperature environment coupled with dust deposition and ice condensation, it is difficult to predict the power production, and, given the role that it assumes in the mission, solutions in terms of software and power

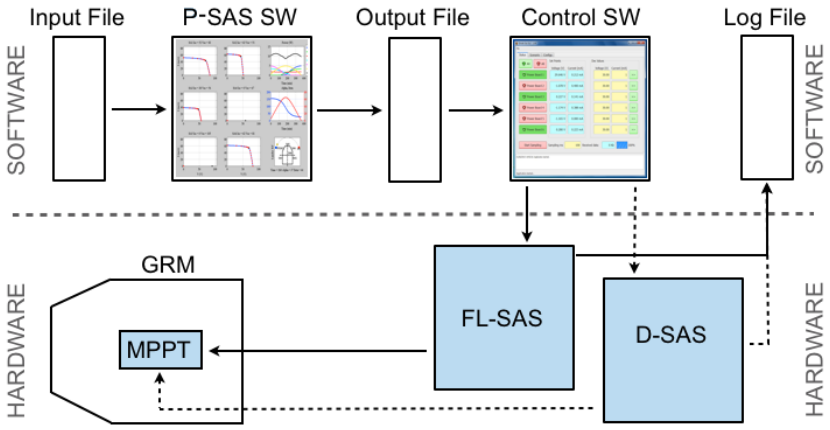

Figure 1.6: SAS Architecture

estimation and simulation are developed.

Politecnico di Milano is participating in the mission development through the Aerospace Engineering Department activities regarding the instrument SD2 (Sampler Drill and Distribution subsystem) and the activities of the Solar Arrays. Ina particular through modeling, simulator ad hoc and development of SW and HW tools to operate the Ground Reference Module (GRM).

The whole simulation system architecture is shown in fig. 1.6. Beside the Philae Solar Array Simulator (PSAS), which will be presented properly in section 1.4, it is possible to see the Fast Loop SAS (FL-SAS) and the Diode SAS (D-SAS).

Required is the Input File, which contains environmental parameters (sun incidence angles, sun distance, SA temperature and fluence) as a function of time. The P-SAS then elaborates the IV curve data for each solar array for every time sample present in the input file. The result is an output file with discretized IV curves and a summary of the simulation.

The Control Software imports the data and is used to operate and set the parameters of the hardware simulators. While FL-SAS uses a union of straight lines to represent the curves, the D-SAS uses a chain of diodes and has no control over the curves shape. At the end of the architecture flow are the Log File, containing the simulation information and summary, and the GRM, equipped with all Philae's subsystems and payloads but the solar arrays. The SAS is connected to the GRM via MPPT.

The Fast Loop SAS The FL-SAS is made up by six electrical boards, each one independent from the others. Each board has a number of programmable potentiometers used to discretize the IV curves into straight lines

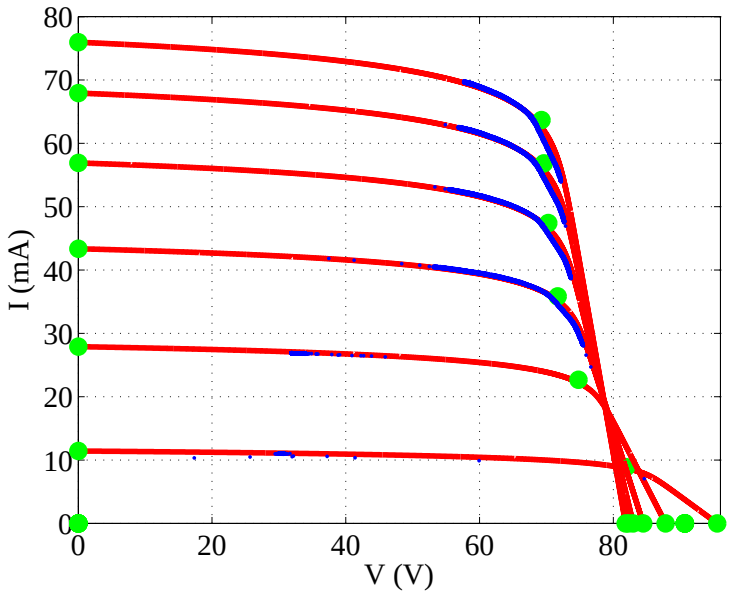

Figure 1.7: IV curves and MPPT sampling [8]

with varying slope. This method is flexible and permits to reproduce cases with variation of maximum power point without a variation of V_{OC} (Open circuit voltage) and I_{SC} (Short circuit current).

The Diode SAS The D-SAS has six independent electrical channels, and the IV curves are represented by a chain of diodes connected in series. The limitations for this solution are in general the dependency of the curves from the diodes performance and temperature. For these reasons the D-SAS is used as back-up simulator. As the FL-SAS is chosen to operate with the GRM, the connection to the MPPT is crucial. Tests have been done by connecting the two hardware and the conclusion is that the conjunction is successful, giving the chance to see how the MPPT sampled values are located on the theoretical curves. The fig. 1.7 shows also how it works smoothly on the MPP (maximum power point) range and how for low currents it stops tracking and starts the ”pass through” mode, where there is no power tracking and the power production is directly poured in the electrical bus.

1.4 PSAS Phiale Solar Array Simulator

P-SAS is a program package written in Matlab language, and it is created to define proper IV line curves as input for the hardware simulator to in-

terface with GRM [8]. Developed at the Aerospace Engineering Department of Politecnico di Milano, it is designed to compute the performances of the six solar arrays of lander Philae once the environmental conditions are specified. The program is presented separately from the rest of the SAS given the fundamental role played by it in the development of this thesis.

The main program is capable of solving the non linear function that link the Sun incidence angles to the electrical energy produced by the LILT cells forming the lander SA system. It is written as a function, giving the opportunity to call it from the command window by typing PSAS, and requires the user to provide the input file, which mus be formatted as in fig. 1.8. All the variables present in the input file, needed to solve the problem and previously defined, are here listed:

- **Time** Simulation Time
- **Alpha** Sun azimuth angle
- **Beta** Sun elevation angle
- **Distance** distance from Sun
- **Temp(j)** temperature of SA(j) (j=1, ... , 6) (function of Sun incidence angles and distance from the sun)
- **Fluence** cumulated equivalent radiation dose of 1 MeV (fruntion of time flight)
- **OutputFileName** name of output file

The IV curves, elaborated by PSAS for every time instant given in the input file, are presented in a matrix of figures refreshed as the simulation run, where is possible to see:

- **SA(j)** I_{SC}**,** V_{OC}, IV curve data foe SA(j) (j=1, ... , 6)
- **Power (W)** Total production power from all MPP
- **Alpha, Beta** Sun angles in Philae Reference System
- **Planar Sketch** current position of the Sun in the simulation run, with sunrise and sunset points

The results of PSAS simulation are the output files created in the program main directory: a summary file with information regarding main parameters of the simulation, main features on power production and power produced

Time	Alpha	Beta	T1	T2	T3	T4	T5	T6	Distance	Fluence	OutputFileName
min	deg	deg	C	C	C	C	C	C	AU	10^14 MeV	PhilaePowerTest*
0	154.45	4.73	-130	-130	-85.86	-49.91	-52.12	-106.2	3	5	
4.9968	154.34	6.89	-130	-130	-85.72	-49.87	-52.16	-104.48			
9.9936	154.2	9.04	-130	-130	-85.52	-49.83	-52.22	-102.77			
15.005	154.01	11.2	-130	-130	-85.26	-49.77	-52.3	-101.07			
20.002	153.78	13.3	-130	-130	-84.95	-49.71	-52.4	-99.387			
24.998	153.51	15.5	-130	-130	-84.58	-49.63	-52.52	-97.722			
29.995	153.19	17.6	-130	-130	-84.15	-49.53	-52.66	-96.078			
35.006	152.83	19.7	-130	-130	-83.66	-49.43	-52.82	-94.458			
40.003	152.41	21.9	-130	-130	-83.1	-49.32	-53.01	-92.865			
45	151.94	24	-130	-130	-82.48	-49.19	-53.23	-91.302			
49.997	151.41	26.1	-130	-130	-81.79	-49.05	-53.48	-89.772			
54.994	150.82	28.2	-130	-130	-81.03	-48.9	-53.77	-88.277			
60.005	150.16	30.3	-130	-130	-80.2	-48.75	-54.09	-86.82			
65.002	149.43	32.3	-130	-130	-79.29	-48.58	-54.47	-85.402			
69.998	148.62	34.4	-130	-130	-78.29	-48.4	-54.9	-84.028			
74.995	147.72	36.4	-130	-130	-77.22	-48.22	-55.38	-82.699			
80.006	146.73	38.4	-130	-130	-76.05	-48.04	-55.94	-81.418			
85.003	145.64	40.4	-130	-130	-74.8	-47.85	-56.58	-80.186			
90	144.44	42.4	-130	-130	-73.45	-47.67	-57.32	-79.006			
94.997	143.1	44.3	-130	-130	-72.01	-47.49	-58.18	-77.879			
99.994	141.63	46.2	-130	-130	-70.48	-47.33	-59.17	-76.809			
105	140.01	48	-130	-130	-68.85	-47.19	-60.32	-75.797			
110	138.21	49.8	-130	-130	-67.13	-47.08	-61.67	-74.844			

Figure 1.8: PSAS input file [8]

by the six SA, total power, alpha and beta at each time label (an example in fig. 1.10); 6 sample detailed files, one for every solar array, containing quantities at each time label as Voc, Vmp, Imp and Isc (an example for SA5 in fig. 1.11).

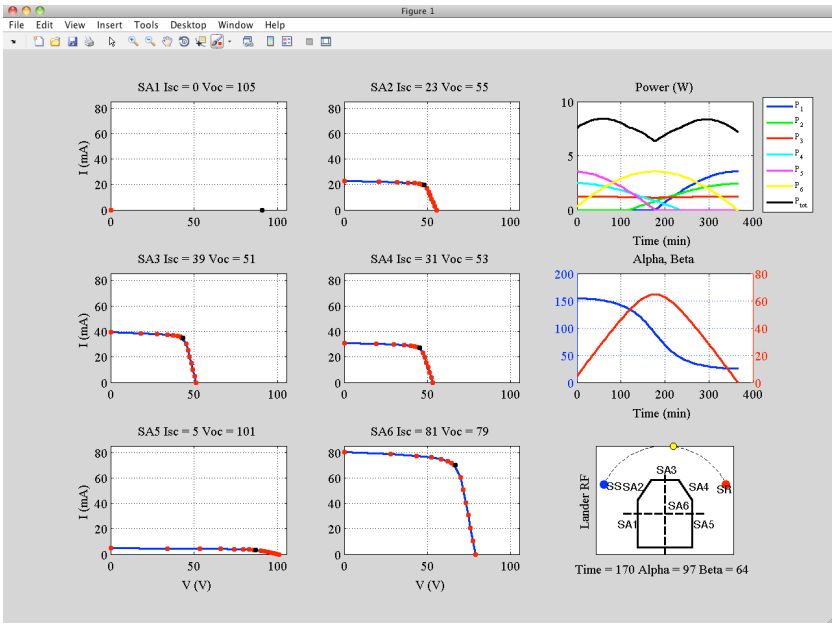

Figure 1.9: PSAS matrix figure [8]

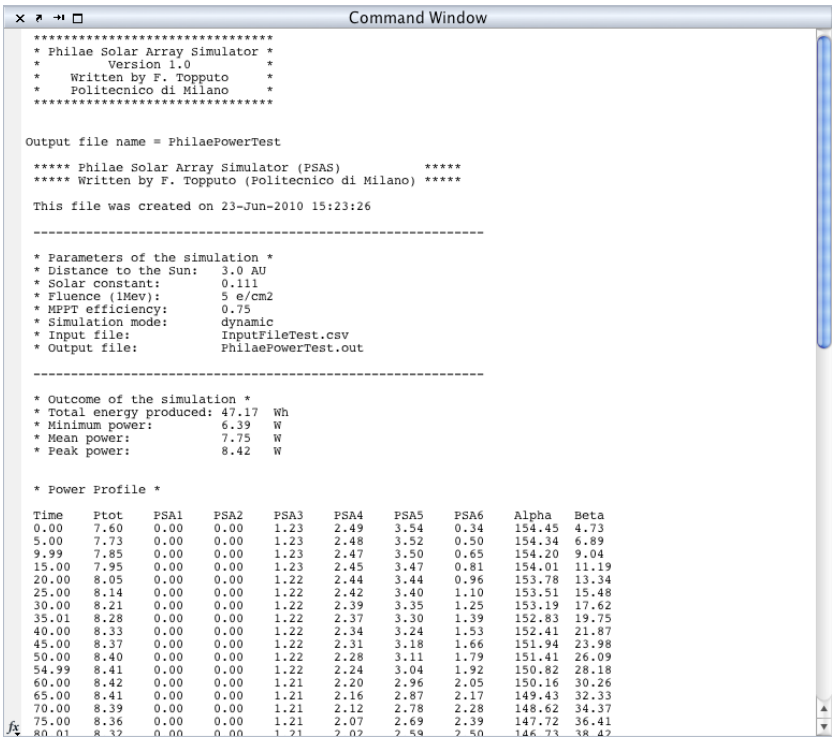

Figure 1.10: PSAS summary file [8]

```
1  ***** Philae Solar Array Simulator (PSAS)           *****
2  ***** Written by F. Topputo (Politecnico di Milano) *****
3
4   Input file: InputFileTest.csv
5
6   This file was created on 23-Jun-2010 15:23:27
7
8  Note: Currents are in mA.
9
10  ***** SA5 *****
11
12  Time     Voc      Vmp      Imp      Isc
13  0.00     81.75    68.97    68.39    81.43
14  5.00     81.77    68.98    68.06    81.04
15  9.99     81.79    69.00    67.61    80.51
16  15.00    81.81    69.02    67.04    79.84
17  20.00    81.84    69.05    66.35    79.03
18  25.00    81.87    69.08    65.54    78.08
19  30.00    81.92    69.12    64.62    77.00
20  35.01    81.97    69.17    63.57    75.77
21  40.00    82.02    69.22    62.42    74.42
22  45.00    82.09    69.28    61.15    72.93
23  50.00    82.16    69.35    59.77    71.31
24  54.99    82.25    69.43    58.29    69.57
25  60.00    82.35    69.52    56.70    67.71
26  65.00    82.46    69.62    55.00    65.72
27  70.00    82.59    69.74    53.21    63.62
28  75.00    82.73    69.88    51.32    61.41
29  80.01    82.90    70.03    49.34    59.08
30  85.00    83.09    70.21    47.26    56.65
31  90.00    83.32    70.42    45.10    54.12
32  95.00    83.57    70.65    42.86    51.50
33  99.99    83.87    70.93    40.53    48.78
34  105.00   84.21    71.25    38.14    45.98
35  110.00   84.62    71.62    35.67    43.09
36  115.00   85.09    72.06    33.13    40.12
37  120.00   85.65    72.58    30.54    37.09
38  124.99   86.31    73.19    27.89    33.99
39  130.00   87.09    73.91    25.19    30.83
40  135.00   88.01    74.76    22.46    27.62
41  140.00   89.11    75.78    19.70    24.37
42  144.99   90.41    76.98    16.92    21.09
43  150.00   91.94    78.40    14.14    17.78
44  155.00   93.73    80.06    11.39    14.47
45  160.00   95.81    81.98    8.68     11.16
46  165.00   98.17    84.17    6.04     7.88
47  170.01   100.82   86.61    3.50     4.64
48  175.00   103.71   89.29    1.07     1.45
49  180.00   105.11   90.59    0.00     0.00
50  185.00   105.11   90.59    0.00     0.00
51  189.99   105.11   90.59    0.00     0.00
```

Figure 1.11: PSAS sample data file (SA5) [8]

Chapter 2

Statement of the problem

2.1 Motivations

The main source of power for Philae is the Battery Unit: the Primary Battery (1000 Wh on landing) is capable to support the demand for up to five cometary days, the time needed to feed electrical power to the landere during SDL and FSS. The Secondary battery, 130 Wh at landing, is placed not only as back-up, but has the role to store the power produced by the Solar Arrays to extend the mission life, giving the chance to gather more data from the comet during the LTS phase [8].

The electrical energy the solar arrays are capable to produce depends on cells characteristics and environmental conditions: some increase the power productions, as the working temperature, other decrease it, as dust deposit, ice formation and cumulated radiation dose. With environmental conditions assigned, the power production depends on solar flux, which decreases with the inverse of the square distance from the sun, and the sunlight incidence on the solar panels. Since the first is imposed by the comet orbit, the attention is focused on the latter .

The ability to increase the power production not only gives the chance to maintain the system alive, but also, if the generation is higher enough with respect to consumption, the opportunity to accomplish more scientific experiments during LTS operative phase. This reason enforces to operate at solar incidence angles that maximize the total power produced by the whole generator.

Previous studies [9] show that the direction capable to achieve such result during cometary day is where Wall 3, namely the x axis in Philae body reference system, is directly oriented towards the sun culmination, independently from the elevation of the Sun (fig. 2.1).

Exception to this configuration is when occurs the phenomenons defined

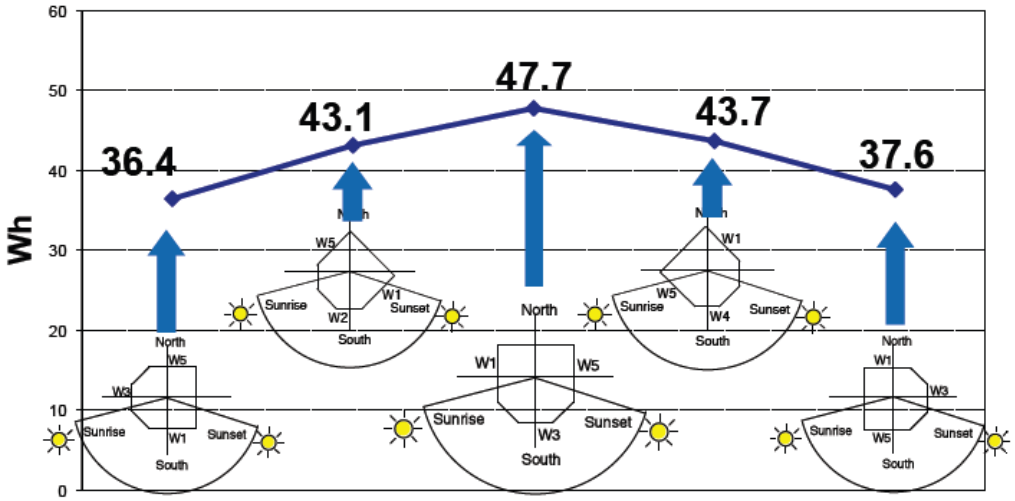

Figure 2.1: Orientation to achieve optimal power production [9]

as Hovering and Zenith transit. During Hovering the Sun never sets, being visible all the time, and the best orientation is where the Wall 3 is oriented towards the direction of minimum Sun elevation: usually when there is sunset it is important to exploit each single solar array panel during the day, leaving the back of Philae, the only wall without SA, to watch the segment of horizon facing the deep space; but when it is always visible this requirements decays and it is better to ensure that the Sun is nearer most of the time to the perpendicular of the single panels during the cometary day.

Instead when Zenith transition occurs it is important to exploit the half of the hemisphere where is located the parable of the Sun, as this ensure to point wall3 to where the Sun is during the day.

2.2 Philae Attitude

Due to strict mass limitations, the lander Philae does not have any system for attitude determination, and the lack of on board instrument assigned to this job make it difficult an identification of Sun location during the cometary day and the lander orientation with respect to it. The only allowed attitude control is the ability to rotate around the zenith axis. The need to save power for scientific research and lander survivability demands a single finite rotation to maximize power production in a long term period.

All these aspects urge to find methods to collect data on Sun direction through alternative ways using only the devices available on board. In addic-

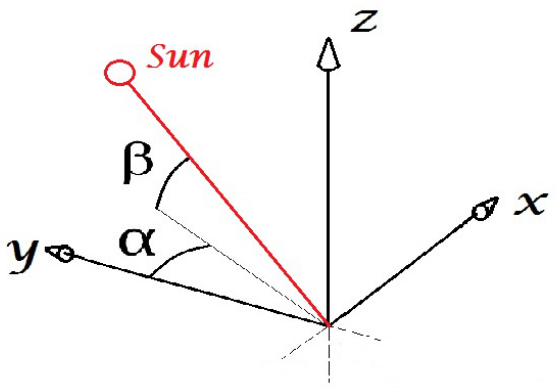

Figure 2.2: Alpha and Beta angles in Philae Body reference system

tion to this, all the information must be transmitted to command center for the computational process needed to obtain the corrective manoeuvre, which must be then transmitted back: given the delay occurring during telecommunications is impossible to gather information by directly operating the lander on comet.

As the power production is a non linear function of sunlight incidence on the solar arrays, a solution to the problem is the reconstruction of Sun direction through the PSS telemetry. Known the model of the phenomenon, and set the contour variables, it is possible to derive the value that defines the output data: in this case the idea is to obtain the Sun angle over the solar array from the MPPT current output. Not only this approach operates directly on the quantity intended to be maximized, it demands no more data those already allocated to be transmitted to control center, as the information needed is already stored in the telemetry required to check the lander status.

2.2.1 Alpha and Beta: Sun Incidence Angles

The Sun incidence angles α and β are used to define the Sun orientation inside the lander body reference system. At each time instant this pair of angles univocally set the components of the Sun versor s along the x, y and z axis shown in fig. 1.5.

The alpha angle, α, is defined as the horizontal angle measured clockwise from the Y axis to the perpendicular projection of the star down onto the local horizon, the XY plane, similarly to the azimuth angle in spherical coordinate system. In the same way the beta angle, β, is defined likely to the elevation angle, and represents the angle between the Sun and the local horizon. An example is shown in fig. 2.2.

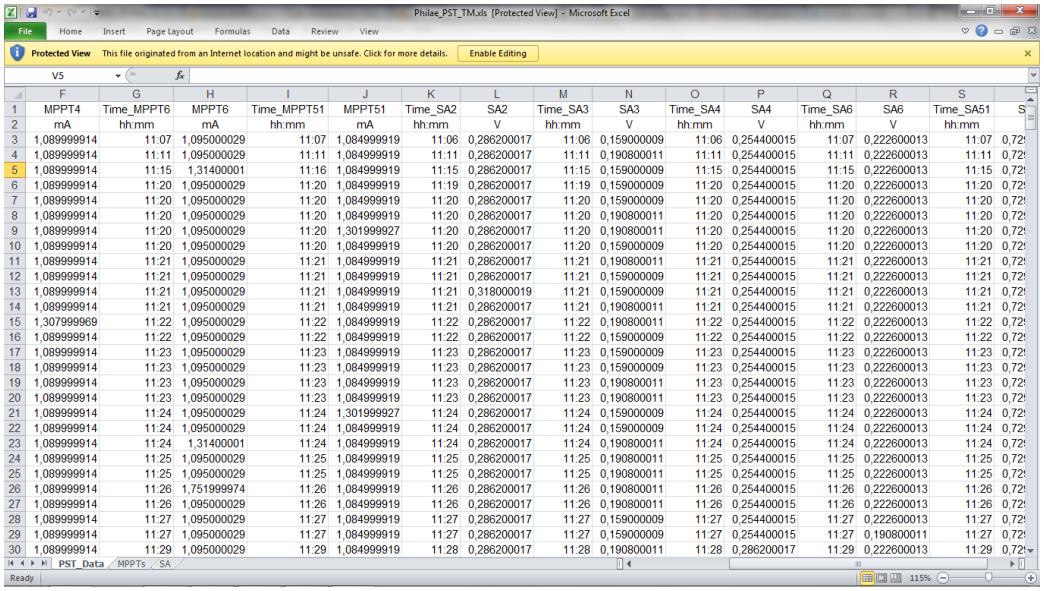

	F	G	H	I	J	K	L	M	N	O	P	Q	R	S
1	MPPT4	Time_MPPT6	MPPT6	Time_MPPT51	MPPT51	Time_SA2	SA2	Time_SA3	SA3	Time_SA4	SA4	Time_SA6	SA6	Time_SA51
2	mA	hh:mm	mA	hh:mm	mA	hh:mm	V	hh:mm	V	hh:mm	V	hh:mm	V	hh:mm
3	1,089999914	11:07	1,095000029	11:07	1,084999919	11:06	0,286200017	11:06	0,159000009	11:06	0,254400015	11:07	0,222600013	11:07
4	1,089999914	11:11	1,095000029	11:11	1,084999919	11:11	0,286200017	11:11	0,190800011	11:11	0,254400015	11:11	0,222600013	11:11
5	1,089999914	11:15	1,31400001	11:16	1,084999919	11:15	0,286200017	11:15	0,159000009	11:15	0,254400015	11:15	0,222600013	11:15
6	1,089999914	11:20	1,095000029	11:20	1,084999919	11:19	0,286200017	11:19	0,159000009	11:20	0,254400015	11:20	0,222600013	11:20
7	1,089999914	11:20	1,095000029	11:20	1,084999919	11:20	0,286200017	11:20	0,159000009	11:20	0,254400015	11:20	0,222600013	11:20
8	1,089999914	11:20	1,095000029	11:20	1,084999919	11:20	0,286200017	11:20	0,190800011	11:20	0,254400015	11:20	0,222600013	11:20
9	1,089999914	11:20	1,095000029	11:20	1,301999927	11:20	0,286200017	11:20	0,190800011	11:20	0,254400015	11:20	0,222600013	11:20
10	1,089999914	11:20	1,095000029	11:20	1,084999919	11:20	0,286200017	11:20	0,159000009	11:20	0,254400015	11:20	0,222600013	11:20
11	1,089999914	11:21	1,095000029	11:21	1,084999919	11:21	0,286200017	11:21	0,190800011	11:21	0,254400015	11:21	0,222600013	11:21
12	1,089999914	11:21	1,095000029	11:21	1,084999919	11:21	0,286200017	11:21	0,159000009	11:21	0,254400015	11:21	0,222600013	11:21
13	1,089999914	11:21	1,095000029	11:21	1,084999919	11:21	0,318000019	11:21	0,159000009	11:21	0,254400015	11:21	0,222600013	11:21
14	1,089999914	11:21	1,095000029	11:21	1,084999919	11:21	0,286200017	11:21	0,190800011	11:21	0,254400015	11:21	0,222600013	11:21
15	1,307999969	11:22	1,095000029	11:22	1,084999919	11:22	0,286200017	11:22	0,190800011	11:22	0,254400015	11:22	0,222600013	11:22
16	1,089999914	11:22	1,095000029	11:22	1,084999919	11:22	0,286200017	11:22	0,159000009	11:22	0,254400015	11:22	0,222600013	11:22
17	1,089999914	11:23	1,095000029	11:23	1,084999919	11:23	0,286200017	11:23	0,159000009	11:23	0,254400015	11:23	0,222600013	11:23
18	1,089999914	11:23	1,095000029	11:23	1,084999919	11:23	0,286200017	11:23	0,159000009	11:23	0,254400015	11:23	0,222600013	11:23
19	1,089999914	11:23	1,095000029	11:23	1,084999919	11:23	0,286200017	11:23	0,190800011	11:23	0,254400015	11:23	0,222600013	11:23
20	1,089999914	11:23	1,095000029	11:23	1,084999919	11:23	0,286200017	11:23	0,190800011	11:23	0,254400015	11:23	0,222600013	11:23
21	1,089999914	11:24	1,095000029	11:24	1,301999927	11:24	0,286200017	11:24	0,159000009	11:24	0,254400015	11:24	0,222600013	11:24
22	1,089999914	11:24	1,095000029	11:24	1,084999919	11:24	0,286200017	11:24	0,159000009	11:24	0,254400015	11:24	0,222600013	11:24
23	1,089999914	11:24	1,31400001	11:24	1,084999919	11:24	0,286200017	11:24	0,190800011	11:24	0,254400015	11:24	0,222600013	11:24
24	1,089999914	11:25	1,095000029	11:25	1,084999919	11:25	0,286200017	11:25	0,190800011	11:25	0,254400015	11:25	0,222600013	11:25
25	1,089999914	11:25	1,095000029	11:25	1,084999919	11:25	0,286200017	11:25	0,190800011	11:25	0,254400015	11:25	0,222600013	11:25
26	1,089999914	11:26	1,751999974	11:26	1,084999919	11:26	0,286200017	11:26	0,190800011	11:26	0,254400015	11:26	0,222600013	11:26
27	1,089999914	11:26	1,095000029	11:26	1,084999919	11:26	0,286200017	11:26	0,190800011	11:26	0,254400015	11:26	0,222600013	11:26
28	1,089999914	11:27	1,095000029	11:27	1,084999919	11:27	0,286200017	11:27	0,159000009	11:27	0,254400015	11:27	0,222600013	11:27
29	1,089999914	11:27	1,095000029	11:27	1,084999919	11:27	0,286200017	11:27	0,159000009	11:27	0,254400015	11:27	0,190800011	11:27
30	1,089999914	11:29	1,095000029	11:29	1,084999919	11:28	0,286200017	11:28	0,190800011	11:28	0,286200017	11:29	0,222600013	11:29

Figure 2.3: Typical Telemetry file layout

2.3 Power Telemetry

An example of PSS telemetry is shown in fig. 2.3. This is obtained from a power system test during the status check occurred at 1.57 AU on 24th February 2010. It presents the reference layout to use during the development of this thesis, and avoids the search of the power data from the whole telemetry file.

In detail the data is arranged in the following way:

- **PST_Data Worksheet** Here are all the informations regarding PSS telemetry. Each MPPT present a column of Sampling Time [s] and relative value of Current Output [mA] in the first section of the sheet, Sampling Time [s] and relative Voltage Input [V] in the second one. Remembering SA1 and SA5 share the same maximum power point tracker, the MPPTs are organized in the following way: 2, 3, 4, 6, 5+1.

- **MPPTs Worksheet** Here is shown the graph with the MPPT current outputs. It is reported in fig. 2.4.

- **SA Worksheet** Here is shown the graph with the MPPT voltage input, It is reported in fig. 2.5.

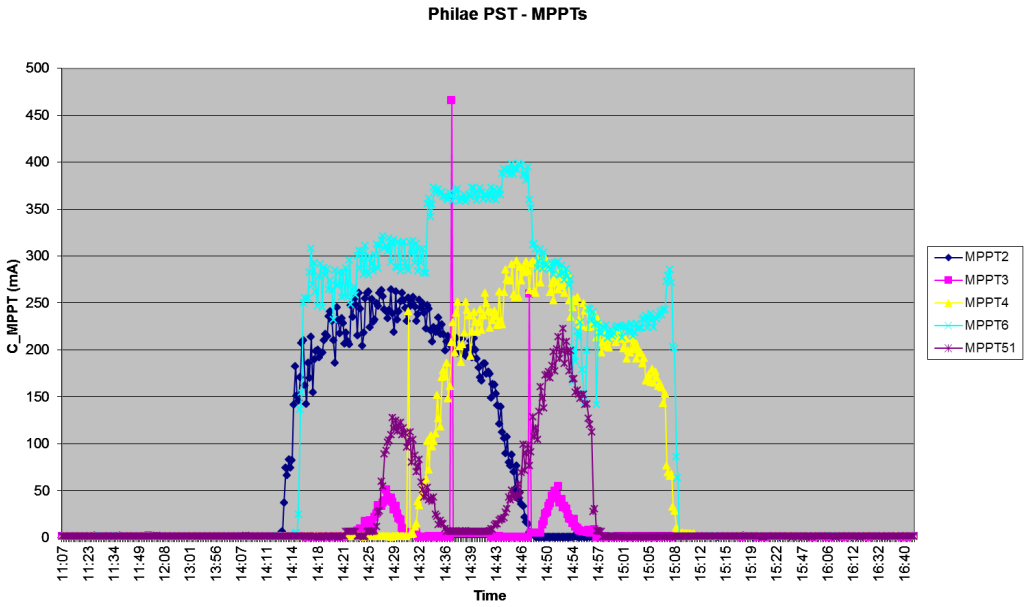

Figure 2.4: MPPT current output

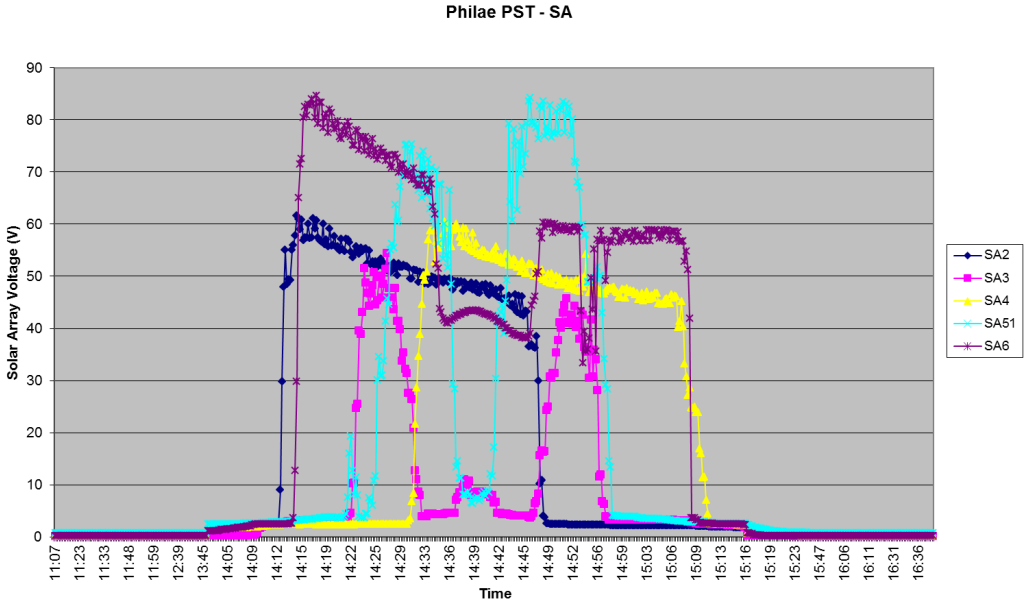

Figure 2.5: MPPT voltage input

2.4 Statement of the Problem

The objective of this thesis is to find the Sun angles, azimuth and elevation, in Philae body reference system, so to obtain the orientation with respect to the Sun during the cometary day, to maximize the power production in the long term period.

The relationship that link Sun incidence angles and power production is a non linear function (chapter 1.4). It is therefore possible find a solution only by defining an inverse problem: a parameter estimation problem necessary to compute values based on observations of the system dynamics [10].

The requirement is an algorithm capable of obtaining the Sun incidence angles during the period of time considered in the input file, the PSS telemetry defined as in chapter 2.3: known the model that describes the phenomenon of power generation on the lander Solar Arrays, this procedure should be able to find the variables that produced the telemetry data through an optimization step. The final result must be the rotation required to point towards the direction of power production optimum during the cometary day (chapter 2.1).

Chapter 3

Problem approach

In this chapter all the steps taken to obtain the Sun incidence angles out of the telemetry data file are discussed: from the data acquiring, through the signal cleaning and preprocessing, and finally to the optimization method.

3.1 Assumptions

Before presenting the processes implemented in the algorithm, it is important to underline all the assumptions taken during the development.

Direct Sunlight It is assumed that the only light affecting the power production is the direct sunlight: this means no albedo, light diffusion through a gaseous medium or reflections of any form. The eventual atmosphere arising as the comet get nearer to sun is therefore not considered. Also any form of dust or ice deposition, that would reduce the ratio of sunlight incidence and the performance in conversion to electricity, is not taken in consideration. All this factors can anytime be corrected by changing the overall efficiency value in the algorithm.

Solar Array Area The area involved in the process of sunlight conversion is the total area of the Solar Array panels, given as the sum of the contribution of every single cell. In case a cell is broken the single array would keep working, unless the number of faulty cells is higher enough to shut down the whole cell string: the active panel area is then reduced. If the number of faulty cells is known it is possible to change the functioning cell number in the program.

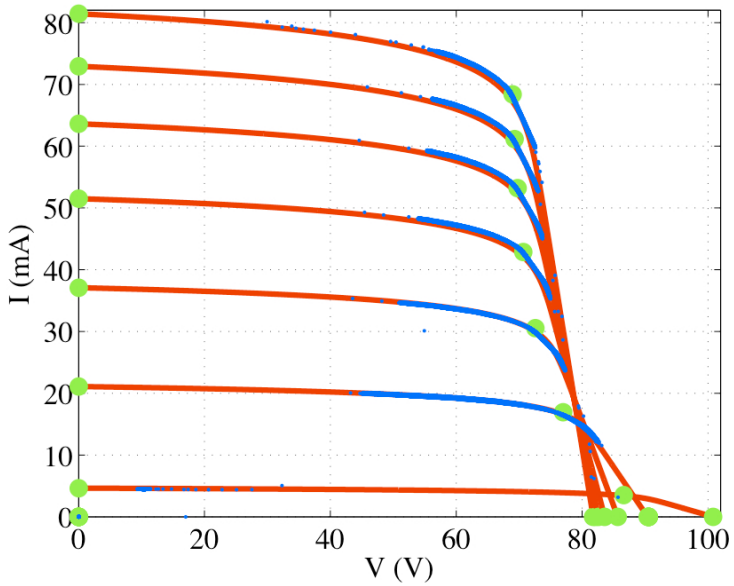

Figure 3.1: MPPT range (blue) on IV cruves (red) [8]

Landing site morphology The landing site is hypothesized as a plane, with no hills, valleys or any sort of obstacles that could project shadows on the SA panels. The inclination of the lender respect the local normal is assumed as zero. Eventual slope on landing site means different beta angles on sunrise and sunset, by default set as zero.

MPPT simulator The telemetry file provided by DLR is from a check test during mission flight, and while it is useful to understand the general behavior of MPPT current output signal and the possible distortions on it, it does not represent an useful example for the purpose of this thesis project. In order to obtain current outputs during a cometary day, a program capable to simulate the behavior of the lander MPPTs has been developed, where the inputs are Sun alpha and beta angles during a defined period of time.

The basis of the program is PSAS, the program presented in chapter 1.4: it is added a random factor on the current output, and the relative voltage is computed. After an analysis of the range the tracker covers on the IV curves, it is chosen a random value for the current that goes from 35% to 75% of I_{SC} (where SC stands for short circuit). It is possible to see the MPPT range in fig. 3.1.

As the bus is set on 28 V, the current conversion happens through the

following formula:

$$Y_j = \frac{V_{out} \cdot I_{out}}{28} \tag{3.1}$$

The alpha and beta angles are obtained from [11], and all possible cases concerning lander location on the comet are covered thanks to 26 histories, spanning a full cometary day. Mainly there are 4 different possible situations:

- **Regular day** there are sunrise and sunset directions($0 < \beta < 90°$), with the presence of night in which the Sun is not visible ($\beta = 0$)
- **Hovering** the Sun never sets, being always visible ($\beta > 0$ always)
- **Zenith Transit** the Sun reaches the zenith ($\beta = 90°$) while the azimuth present a jump of 180°
- **Perpetual night** the sun never rises ($\beta = 0$).

3.2 Preprocessing

All the initial management of the telemetry data is here discussed. Before the optimization process all the needed information must be acquired, eventually cleaned from spurious behaviors and analyzed to identify the power production periods.

3.2.1 Program Lunch & Data Acquiring

The program that implements the algorithm is written as a function so to be called directly form the Matlab Command Window by typing the command "albe". It is possible to load the telemetry file via the dialog box shown in fig. 3.2: the file extension requirede is "*.xls", specified as in chapter 2.3. The file, to be correctly loaded, must be placed inside any directory of the program main folder.

Only the current outputs and relative sampling times will be loaded in the program, as those are the only information needed to find the sun incidence angles. Looking at fig. 2.3 it is possible to see the data disposition: from the first columns of the telemetry file there will be created vectors containing the current samples of panels 2, 3, 4, 6 and for last panels 1 and 5 combined together, each one sided by the corresponding time vector. From now on t_j will represent the time label, where j stands for the cell location inside the vector, and Y_j the corresponding current output.

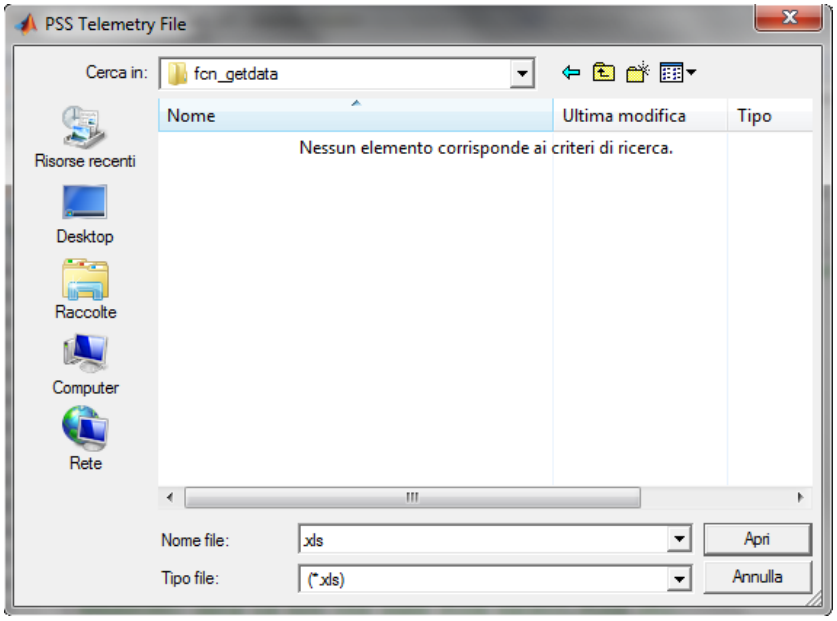

Figure 3.2: Dialog Box to load telemetry file

3.2.2 Frequency Cleaning - Smoothing

Paying attention to the telemetry file showed in chapter 2.3, once the data is properly loaded, it is possible to see that the signals of the current outputs present spurious frequencies due to the MPPT scanning around the maximum power point. On top of that, there are signal spikes plausibly caused by sunlight reflections on other surfaces. A cleaning is urged in order to arrange the signals to be used during sun incidence extrapolation.

Background Definition The first thing to define is the background noise apart from the signal output due to sunlight conversion in electrical power. By analyzing the telemetry file provided by DLR it is defined a rumor of 10 mA: this value is chosen by looking at the maximum value reached when Philae is in shadow and adding some margin to it. The background noise value helps also to determine the time laps in which the single panel is lighted, giving the opportunity to define time windows of power production, as described later on.

Spike Cleaning Eventual spikes in the signal must be cleared: as the signal is not smooth it is difficult to determine when a spike is due to external factors or to MPPT scanning. To solve the problem it is used the probability distribution approach applied to the signals. It is possible to see an example

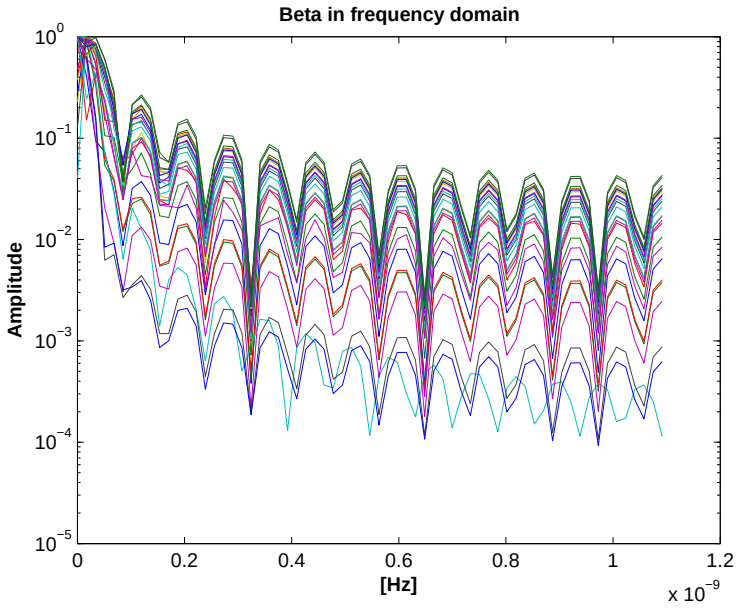

Figure 3.3: Beta angle during cometary day in frequency domain

of such spikes by looking at the current output of MPPT number 3 in fig. 2.4.

It is calculated the mean value and the variance for 5 values centered around the sample of interest: when the local deviation is higher than 2.5 times the variance then it is substituted with the mean value of the adjoining samples. It is possible to change the cutoff value for spikes at any time inside the program.

Frequency cleaning The signals have to be cleaned: one way is to clean the spurious frequencies present in the current output. Using the "fft"with cutoff frequency it is possible to achieve the needed results. The time histories of the Sun incidence angles already in our possession can be converted inside the frequency domain to find of what frequencies are constituted. Beyond these any amplitude contribution can be considered as disturb: this would help in defining the cut off frequency for the current signals, as the MPPT scanning frequencies would fall outside the admissible frequency range. By analyzing examples of cometary day provided by [11], the frequency transposition for beta and alpha are shown in fig. 3.3 and fig. 3.4 respectively.

Each curve represents the transposition in frequency domain of beta and alpha angles in a different location on 67P Churyumov-Gerasimenko during a full cometary day: it is possible to notice the absence of dominant frequencies, and that almost all the domain is covered. This is due to the small orientation

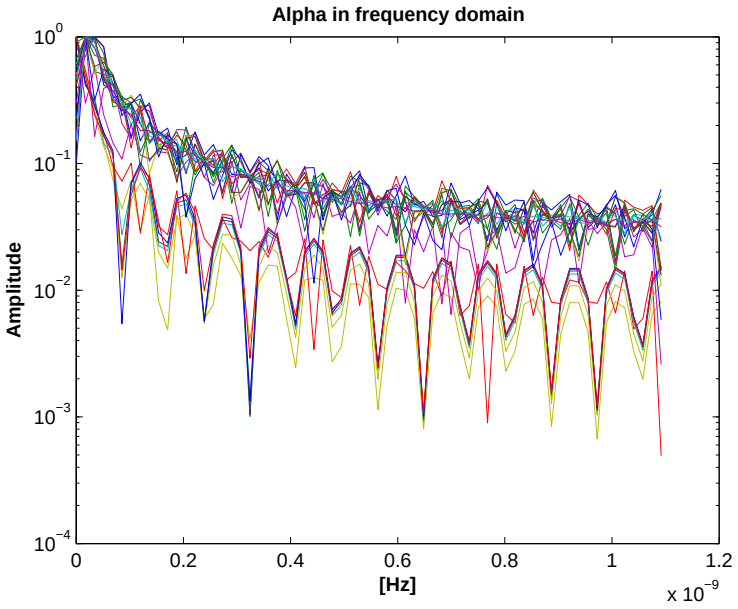

Figure 3.4: Alpha angle during cometary day in frequency domain

variation happening as the comet travels around the Sun, giving the effect on the single day of a gap between starting value and the ending one. This drives the need to find an alternative solution.

Smoothing As the sampling of the current outputs happens at around every 4:15 min ($3.9 \cdot 10^{-3}$ [Hz]) and the frequency at which the MPPTs operate is between 40 and 60 [Hz], it is not possible to determine a common behavior in the signal, giving back the effect of a random noise on the current outputs. A way to reduce such effect is the *smoothing*. In smoothing, the data points of a signal are modified so that individual points that are higher than the immediately adjacent points (presumably because of noise) are reduced, and points that are lower than the adjacent points are increased. This naturally leads to a smoother signal. As long as the true underlying signal is actually smooth, then the true signal will not be much distorted by smoothing, but the noise will be reduced [1]. In the algorithm there are implemented two different smoothing algorithms: the *rectangular* or *unweighted sliding-average smooth* and the *triangular smooth*. In the first method each point is replaced with the average of the m adjacent points, where m is the integer defined as *smooth width*. For a 3 point smooth:

[1] http://terpconnect.umd.edu/ toh/spectrum/Smoothing.html

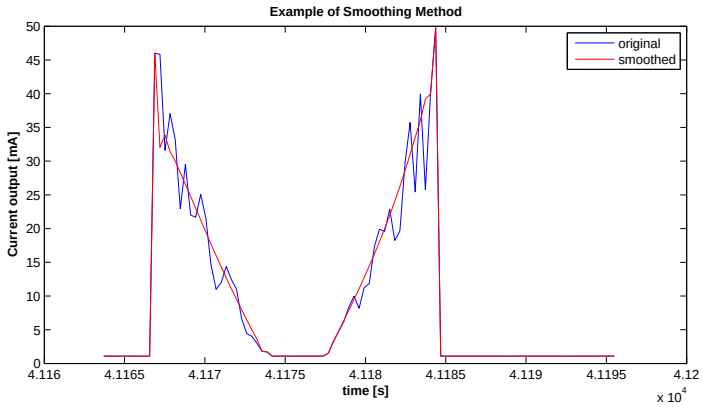

Figure 3.5: Example of *triangular smoothing* (20 times) on a current output

$$S_j = \frac{Y_{j-1} + Y_j + Y_{j+1}}{3} \tag{3.2}$$

for j=1 to n-1, where S is the smoothed signal and Y the original one, and n the total number of signal points. If the noise in the data is "white noise"(that is evenly distributed over all frequencies and actually resemble our case) and its standard deviation is s, then the standard deviation of the noise remaining in the signal after the first pass of an unweighted sliding-average smooth will be approximately s over the square root of m ($s/sqrt(m)$), where m is the smooth width.

The *triangular smooth* is similar except it implements a weighted smoothing function. For m=5

$$S_j = \frac{Y_{j-2} + 2Y_{j-1} + 3Y_j + 2Y_{j+1} + Y_{j+2}}{9} \tag{3.3}$$

for j=2 to n-2. This is equivalent to two passes of a 3-point rectangular smooth. This smooth is more effective at reducing high-frequency noise in the signal than the simpler rectangular smooth. An example of application of smoothing is shown in fig. 3.5.

It is possible to use any of the two inside the algorithm, and the more times the smoothing is applied the more the signal looses behaviors due to the random noise: it is recommended a total of 20 smoothing repetitions as less than 10 is not enough and more than 30 lose efficiency. The chosen value in the algorithm is 30. The *triangular smoothing* is the main choice but it is possible anytime to change to the cleaning in frequency domain, and it is even possible to apply both methods.

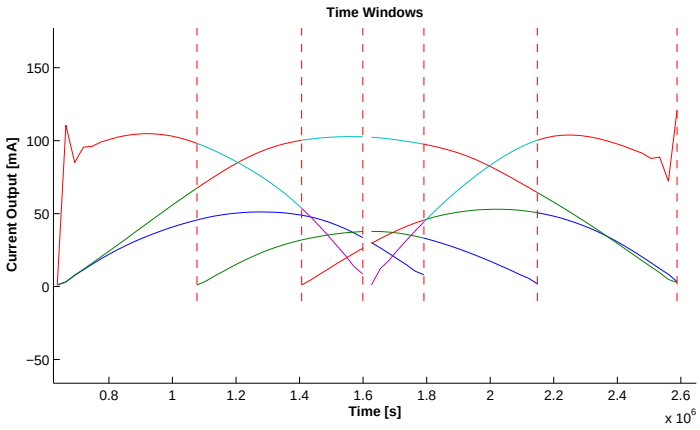

Figure 3.6: Example of Time Windows during a cometary day

3.2.3 Time reference & Time windows

The determination of the sun incidence angles depends on the combination of lighted panels. As only some panels can be lighted in a certain period, it is important to identify intervals of time samples, defined as time windows, where only some arrays are actually working: these windows begin and end as one or more panels start or stop to work. These windows include time samples in which only a certain combination of panels are producing a relevant current output, where others with less significant output are discarded. Eventual windows composed of only two time samples are discarded as too short for any purpose: no information is lost as every window share the contour data. It is possible to see an example of time production segmentation in time windows in fig. 3.6.

Each current output signal has different sampling timing: the data logger acquires the output from a single MPPT and has to rotate between them. The time windows, to be correctly defined, need all the samples to refer at the same time vector: it is required to interpolate the values to a single time reference for the whole SA system.

The linear interpolation is the method chosen, using the command "interp1 ". The extrapolation works for points inside the interval spanned by the original vector. It is taken the reference time as the panel 2 sampling time vector, being the first to be sampled at each cycle, but for the first value of the time reference vector $\mathbf{t}$ it is used the greatest value inside the first sampling time cycle: this is to avoid possible problems by interpolating out of defined intervals and to ensure the only use of gathered information.

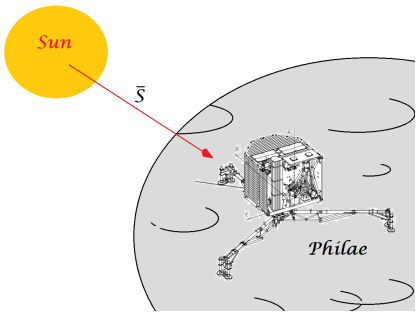

Figure 3.7: Example of Sun vector direction with respect to lander Philae

3.3 First Guess Definition

In order to achieve a faster conversion and to avoid possible local minima during the optimization process, it is needed a starting solution capable to represent, with decent approximation, the value of the problem's solution. The first guess for Sun incidence angles will be computed from the current output through a linear solution, since it is not required a method capable to extrapolate the exact value: all the non linear effects will be included inside the efficiency coefficient. Anyway, the non linear effects will be properly considered inside of the optimization method.

The alpha and beta angles of the Sun direction in Philae reference body system are obtainable from the Sun vector composed by three components: S_x, S_y, S_z. The Sun vector $\mathbf{S}$ is defined as the vector that connect the Star to the lander fig. 3.7.

The general scalar equation for the power output for a lighted solar array is the following:

$$P = V\, I = \mathbf{S} \cdot \mathbf{n}\, A\, \eta \tag{3.4}$$

where:

- P: power output at maximum power point over the curve IV
- V: voltage at maximum power point
- I: current at maximum power point
- **S**: Sun direction vector $\mathbf{S} = S\mathbf{s}$, composed by **s**, Sun versor in Philae reference body system, and sunlight intensity value S, computed as sunlight intensity at Earth (1 AU) divided by the square value of the distance in Astronomical Units
- **n**: solar array panel normal versor

- A: total area of the solar array
- η: total efficiency, includes all the non linear effects, as function of cell conversion efficiency, SA temperature, etc...

The power output is known, as the lander bus voltage is set at 28 V and the current I is the information stored inside the telemetry. Thanks to lander data sheet the total area of every panel and relative normal versor in body reference system are known. In the equation the unknowns are the Sun versor, where S is determined as the distance from the star is defined, and the total efficiency. The objective is the determination of $\mathbf{s}$, from which it is possible to obtain the Sun incidence angles α and β.

As seen before, the Sun direction is composed of three components: therefore a single scalar equation is not enough to determine the three unknowns needed. Therefore it is required to use the information from more panels to write a three equations system capable to solve the problem, demanding that at least 3 panels must lit at the time.

By considering a system of equations we have:

$$\mathbf{P} = 28\,\mathbf{I} = \mathbf{s} \cdot \mathbf{N}\; Diag(\mathbf{A})\; \eta \tag{3.5}$$

where:

- $\mathbf{P}$: vector containing the power outputs
- $\mathbf{I}$: vector of currents of the panels lighted obtained from the telemetry
- $\mathbf{N}$: matrix containing as columns the normals of the panels lighted
- $Diag(\mathbf{A})$: matrix with diagonal the vector of the total area of the lighted solar arrays

To reverse the equation is required the invertibility of $\mathbf{N}$: it must be a square matrix and the combination of lighted panels is such that, being all the panel versors different from each other, at least the panel 6 is included. Otherwise all the versors would be coplanar, leaving the row relating the components along z empty. If panel 6 is not lighted, which almost never happens as usually the sun to be visible must be over the horizon (β=0), the starting guess is not computed. The same happens when only two solar arrays are lighted. Different combinations of panels will be used to compute a mean value so to reduce eventual errors arising from the approximations taken: this will be better discussed later in this chapter.

By reversing the equation, we find:

$$\mathbf{S}_\eta = S\,\eta\,\mathbf{s} = (\mathbf{N}\; Diag(\mathbf{A}))^{-1}\; 28\,\mathbf{I} \tag{3.6}$$

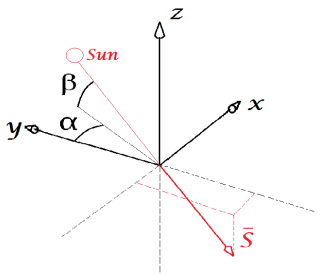

Figure 3.8: Alpha and beta with **s** in Philae body reference system

where $\mathbf{S}_\eta$ is the Sun vector scaled by the total efficiency η. The versor is now obtainable dividing the vector by its modulus:

$$\mathbf{s} = \frac{\mathbf{S}_\eta}{|\mathbf{S}_\eta|} \tag{3.7}$$

In this way the non liner effects are removed, where the only approximation is the allocation of these inside the total efficiency.

The relationship that links power output and sunlight intensity over the solar array depends on the cosine of the angle between panel normal versor **n** and the Sun direction **s**. From the definition seen in fig. 3.7 a panel is lighted when the Sun vector is entering, in other words the scalar product $\mathbf{n} \cdot \mathbf{s}$ gives a negative value: defined θ the angle included between the versors, its value is over 90°. Taking these aspects in mind, and looking at fig. 3.8, the link **s** to α and β is described by the following equations:

$$s_x = -\cos(\beta)\sin(\alpha) \tag{3.8}$$

$$s_y = -\cos(\beta)\cos(\alpha) \tag{3.9}$$

$$s_z = -\sin(\beta) \tag{3.10}$$

Since these are non linear equations a direct revers is not possible, but it still possible to recover alpha and beta thanks to the following system:

$$\alpha = \begin{cases} \arctan\left(\frac{s_x}{z_y}\right) & s_y \geq 0 \\ \arctan\left(\frac{s_x}{z_y}\right) + 180° & s_y < 0 \end{cases}$$

while for β is:

$$\beta = \arcsin(s_z) \tag{3.11}$$

When more than three MPPTs present outputs the first guess problem becomes overdetermined: the number of linearly independent equations m is

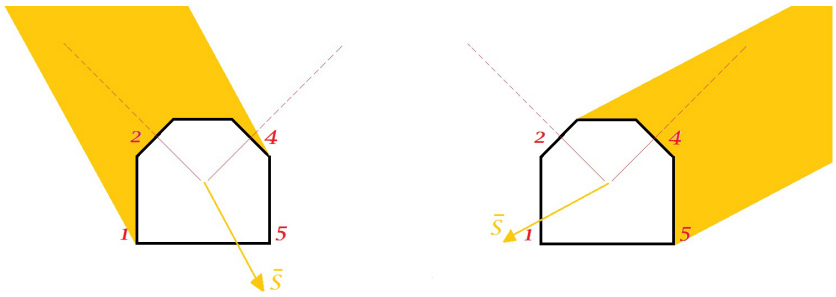

Figure 3.9: Sun direction alignment to panels 2 and 4

greater than the number of unknowns n. To take advantage of such situation it is used a combination system to obtain a series of Sun incidence angle values to lessen the effects of the approximations taken. Fixed the panel 6 needed for the invertibility of $\mathbf{N}$, when the number of lit side walls is more than two, the possible combinations of 2 working MPPTs provide a series of starting guess values α_j and β_j. The starting guess is then taken as the mean values computed in the following way

$$\alpha = \frac{\sum_{j=1}^{n_c} \alpha_j}{n_c} \tag{3.12}$$

$$\beta = \frac{\sum_{j=1}^{n_c} \beta_j}{n_c}, \tag{3.13}$$

where n_c is the number of MPPTs output various combination taken.

A problem arises with the MPPT referring to panel 1 and 5: to figure out which panel is lit it is needed to look to the others. Panel 1 and 5 cannot be lighted simultaneously as they face opposite directions, and since it is possible to determine the angles starting guess only when more than 2 MPPTs are working, the output of MPPT 2 and 4 comes handy.

In fig. 3.9 two possible situations help to determine whether panel 1 or 5 is lit. By diving the α arc in two regions, $-90 \leq \alpha \leq 90$ and $90 < \alpha < 270$, when the MPPT output of panel 2 is higher than panel 4 it means that, on equal SA areas, the Sun direction is more aligned to wall 2 normal: the Sun α is in the first region therefore panel 1 is lighted; on the opposite when panel 4 present higher current output panel 5 is lighted.

3.4 Power system identification as non linear programming problem

Due to the non linear behavior of the phenomenon it is not possible to solve the problem of finding the Sun incidence angles by direct means: it is therefore required to find other ways to achieve such result. A solution is to work with optimization algorithms, specifically with parameter estimation, capable to solve inverse problems as such the one here presented. A parameter estimation problem arises when it is necessary to compute values for these parameters based on observations of the system state[10]: here it is represented by the power output as function of time and the parameters to be estimated are the Sun incidence angles.

3.4.1 Parameter Estimation Problems

Parameter estimation problems are capable to determine the parameters vector of a system $\mathbf{p}$ from the values of the observed state, typically represented from a system of ODEs:

$$\dot{\mathbf{Y}} = \mathbf{f}[\mathbf{Y}(t), \mathbf{u}(t), \mathbf{p}, t] \tag{3.14}$$

for a given time interval $t_i \leq t \leq t_f$, where $\mathbf{Y}$ is the n_Y dimension state vector, $\mathbf{u}$ an n_u vector of algebraic variables and $\mathbf{p}$ are the parameters of the system.

In addition it is possible to define eventual algebraic path constrains, and it is computational useful to include simple linear bounds on the variables:

$$\mathbf{Y}_l \leq \mathbf{Y}(t) \leq \mathbf{Y}_u \tag{3.15}$$

$$\mathbf{u}_l \leq \mathbf{u}(t) \leq \mathbf{u}_u \tag{3.16}$$

$$\mathbf{p}_l \leq \mathbf{p} \leq \mathbf{p}_u \tag{3.17}$$

A difference with optimal control problem, whose objective function involves quantities evaluated continuously over the entire domain, the parameter estimation objective is evaluated at a finite, possibly large, number of discrete points. Unlike classical optimal control problems the goal here is to determine the n_p dimensional vector $\mathbf{p}$ to minimize the performance index:

$$F = \frac{1}{2}\mathbf{r}^T\,\mathbf{r} = \frac{1}{2}\sum_{k=1}^{l} r_k^2 \tag{3.18}$$

$$r_k = w_k \left[y_{i(k)}(\theta_k) - \widehat{y}_{i(k)} \right] \tag{3.19}$$

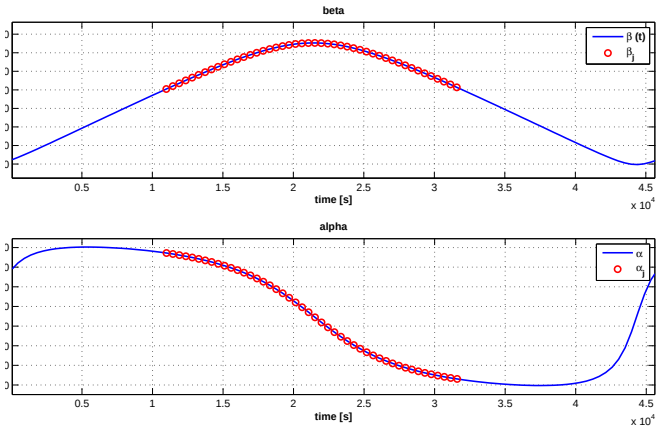

Figure 3.10: Sun incidence angles discrete values during cometary day

where $y_{i(k)}$ is the state variable i computed at time θ_k and $\widehat{y}_{i(k)}$ is the observed value at the same time. The time instant θ_k must satisfy:

$$t_i \leq \theta_k \leq t_f \tag{3.20}$$

3.4.2 Parameter Estimation applied to Sun incidence problem

In order to write the parameter estimation problem we need to define the following conditions that constitute it.

Parameter vector definition Usually the parameters are defined as continuous function of time, so that for any give time $t_I \leq t \leq t_F$ it is defined the couple of angles $\alpha(t)$ and $\beta(t)$ capable to uniquely determine the direction of the Sun in lander body reference system.

However the current outputs present in the telemetry files are sampled at discrete time $t_I \leq t_j \leq t_F$ for $j = 1, \ldots, n$, where $t_I = t_{j=1}$, $t_F = t_{j=n}$ and n is the total number of time samples: the reference time vector $\mathbf{t}$ is constituted as seen in chapter 3.2.3.

The relative Sun incidence angles are therefore a finite number, and we define for each time sample t_j the pair of angles $\alpha_j = \alpha(t_j)$ and $\beta_j = \beta(t_j)$. In fig. 3.10 it is possible to see an example of discrete distribution of Sun incidence angles over the continuous time history, sampled during Sun visibility in the cometary day.

The angles, which are the parameters that define the non linear optimization problem, are gathered inside the parameter vectors $\mathbf{x}$, defined as

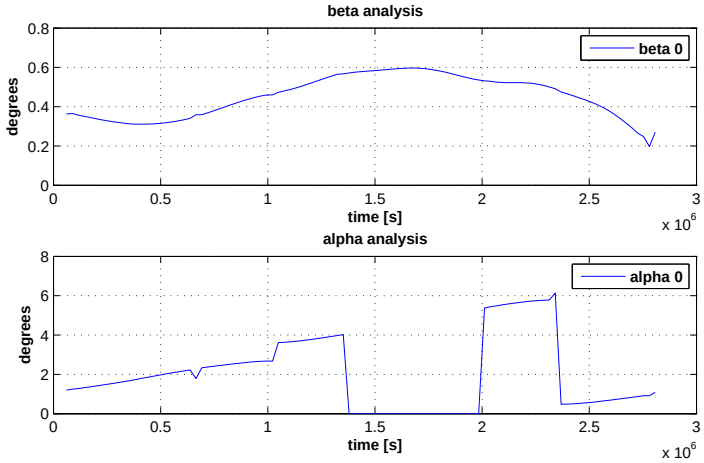

Figure 3.11: First guess example

follow

$$\mathbf{x} = \{\alpha_j, \ldots, \alpha_n, \beta_j, \ldots, \beta_n\}. \tag{3.21}$$

Starting guess $\mathbf{x}_0$ The initial solution may not be accurate but it is useful: other than giving a first look to the trend of the Sun incidence angles it starts the optimization closer to the exact solution, reducing computational time and lowering the chance to find a local minimum. An example is presented in fig. 3.11.

It is possible to notice a gap in the solution for α: as shown in chapter 3.3, $\mathbf{x}_0$ could be computed only when there are more than 2 panels lit, so a gap is present only when wall 1 or 5 is lighted with wall 6. The lack of continuity in the solution will be compensated by the boundary constrains and a first optimization iteration presented later in this chapter.

Boundary constrains Here are defined the boundaries that α and β must respect, as upper (**UB**) and lower (**LB**) bounds. Every wall has a defined azimuth and elevation range inside which it could be lit: as the Sun incidence angles must respect the boundaries for each panel, when more walls are lighted the overlap of constrains defines the arc range to be satisfied.

Since panels 1 and 5 share the same current output and face opposite direction, their range covers from 0° all over to 360°, and therefore are left out from boundary constrains definition. Every combination of lighted panels present the α range shown in tab. 3.1.

Table 3.1: Alpha boundary range

Walls	α Range
0 0 0	$225° \leq \alpha \leq 315°$
2 0 0	$315° \leq \alpha \leq 360°$
2 3 0	$0° \leq \alpha \leq 45°$
2 3 4	$45° \leq \alpha \leq 135°$
0 3 4	$135° \leq \alpha \leq 180°$
0 0 4	$180° \leq \alpha \leq 225°$

Table 3.2: Beta boundary range

Wall	β Range
6	$-10° \leq \beta \leq 90°$

As beta depends mainly from the current output of panel 6, boundary constrains are defined only when the top wall is lighted, and present the range in tab. 3.2. The lower boundary is defined less than zero for two reasons: by giving some flexibility possible wrong behaviors are reduced as beta is near to zero, especially at sunrise and sunset; in case comet horizon is not flat int this way is left some range inside which the sun may transit. It is possible to see an example of boundary constrains in fig. 3.12.

The walls are considered lighted only when their current output exceeds a threshold values, and in some limit cases this drive to slightly constricting boundaries: in general it is possible to solve such problems by loosening the constrains.

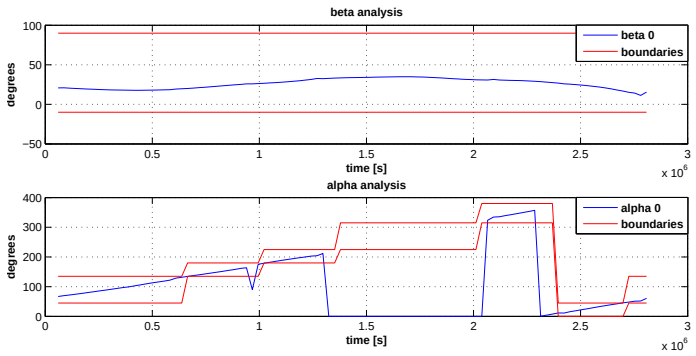

Figure 3.12: Sun Incidence Angles boundary constrains

Non linear constrains This ensure a more strict control on the values that the solution can obtain during the optimization. It is possible to impose a non linear equality constrain between α and β by knowing the Sun direction versor $\mathbf{s}$ components seen in 3.8 to 3.10

$$\mathbf{s}^T\mathbf{s} = s_x^2 + s_y^2 + s_z^2 = 1. \tag{3.22}$$

Therefore the equality non linear constrain can be written in the following way

$$g(\mathbf{x}) = (cos(\beta)sin(\alpha))^2 + (cos(\beta)cos(\alpha))^2 + (sin(\beta))^2 - 1 = 0. \tag{3.23}$$

In general it could be useful to impose constrains on the slope of the angles too: such thing would help to avoid spikes and secure continuity to the solution, but the wide range of values that the slope attains makes it impossible to define specific boundaries. As result it is not defined any limit to the trend behavior of the parameters.

Performance index The solution to a parameter estimation problem requires the minimization of the performance index F, defined as function of the parameters vector $\mathbf{x}$ that returns a scalar value. In order to compute F as seen in section 3.4.1 it is needed to define the residual vector $\mathbf{r}$, which represents the difference between system dynamics outputs $\widehat{\mathbf{Y}}$ and the reconstructed one $\mathbf{Y}$: it must be evaluated for each MPPT output, so it is expressed in the following way

$$\mathbf{r}_i = \mathbf{Y}_i - \widehat{\mathbf{Y}}_i, \tag{3.24}$$

for $i = 1, \ldots, 5$, as many as the MPPT on the lander.

The dependence of the performance index to the parameters vector $\mathbf{x}$ is through the reconstructed MPPT current outputs: this is achieved thanks to the model present in PSAS (chapter 1.3.1), capable to define the current output as function of α and β, wall temperature and total radiation dose. While the last one is a value independent of the sun incidence and must be provided, the wall temperatures depend on the lander orientation: to obtain these it is used the model provided in [12] and here showed

$$T_i = A_i + B_i \frac{SC}{d^2}\cos(\vartheta) + C_i\left[\frac{SC}{d^2}\cos(\vartheta)\right]^2, \tag{3.25}$$

for $i = 1, \ldots, 6$, one for each wall, where $SC = 1346 W/m^2$, d is the distance from the Sun in AU, ϑ is angle between Sun direction versor and wall normal and the coefficients A_i, B_i and C_i are obtained from tab. 3.3.

Table 3.3: Temperature coefficients

	$A_i\,[°C]$	$B_i\,[Km^2/W]$	$C_i\,[Km^2/W^2]$
sunlighted $i = 1, \ldots, 5$	-138	0.7875	-0.001535
in shadow $i = 1, \ldots, 5$	-88	0.4372	-0.000577
wall 6	-109	0.3074	0

Once defined the current outputs the performance index is computed in the following way:

$$F(\mathbf{x}) = \sum_i (\mathbf{Y}_i - \widehat{\mathbf{Y}}_i)^T (\mathbf{Y}_i - \widehat{\mathbf{Y}}_i), \tag{3.26}$$

where $\mathbf{Y}_i$ is the computed current output vector for the i-th wall from the parameter in x, while $\widehat{\mathbf{Y}}_i$ is the relative current output from telemetry.

It is possible to solve each time instant optimization problem independently, since the characteristic times of the variables involved are greatly smaller than the revolution period of the comet: this lead to a model modeled through algebraic equations instead of differential.

However, due to computational time it is preferred to optimize on time lapses bigger than the single time instant: in this way it is possible to solve on a number of samples smaller than the original size, and compute the performance index on the whole power production period through linear interpolation. It is preferred the linear interpolation with respect to spline interpolation or other methods because, even if it does not provide continuity on the slope, it avoids unpredictable trends during the computational process that could drive to divergence. Now the current outputs, for example, are computed on $\mathbf{Y}_k$ for $k = 1, 4, 7, ..., n_Y$, and the performance index is:

$$F(\mathbf{x}) = \sum_i (\bar{\mathbf{Y}}_i - \widehat{\mathbf{Y}}_i)^T (\bar{\mathbf{Y}}_i - \widehat{\mathbf{Y}}_i) \tag{3.27}$$

where $\bar{\mathbf{Y}}_i$ is the current interpolated on the $i - th$ instant from the current outputs in k. This is valid also because the time gap represented by $t_k - t_{k-1}$ is not big enough to permit substantial changes in the Sun incidence angles during the cometary day. In the performance equation the telemetry current outputs must be premultiplied by a correction factor, because the signal clean presented in chapter 3.2.2 provides a mean trend of the current, but the effect of the MPPT mean loss still remain. To avoid problems arising from the discrepancy between solution and telemetry it is added the following term inside the F expression:

$$F(\mathbf{x}) = \sum_i (\bar{\mathbf{Y}}_i - \widehat{\mathbf{Y}}_i/0.8)^T (\bar{\mathbf{Y}}_i - \widehat{\mathbf{Y}}_i/0.8) \tag{3.28}$$

Definition It is now possible to write the nonlinear parameters estimation problem as follow:

$$\min_{LB \leq \mathbf{x} \leq UB} \quad F(\mathbf{x}) \quad \text{subject to} \quad g(\mathbf{x}).$$

3.5 Performance index local minima

To show the behavior of the performance index it is reported in fig. 3.13 the plot of F(x) as function of azimuth α and elevation β computed at a defined sampling time.

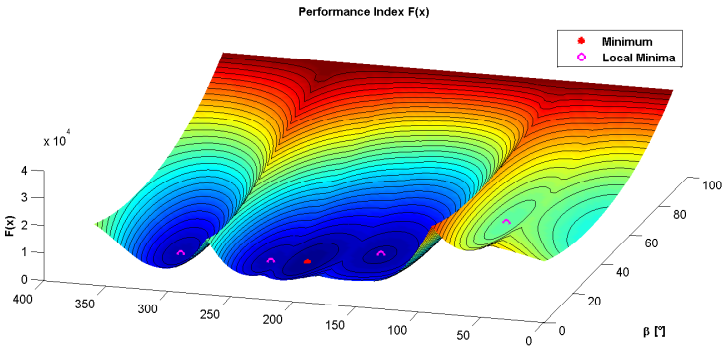

Figure 3.13: Performance index course

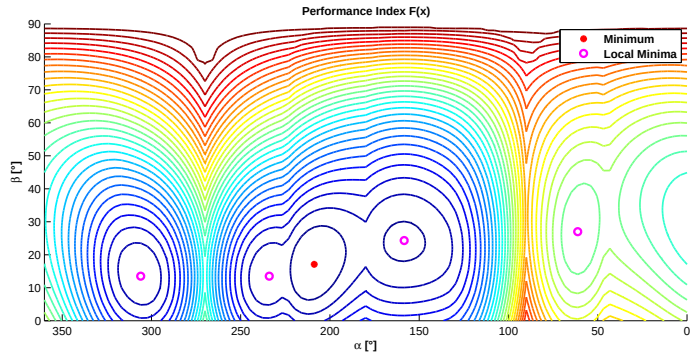

Figure 3.14: Performance index contour course

To show more clearly show the position of the mimima in fig. 3.14 it is presented the contour plot of the same function. By looking to both plots it is clear that not only there's the presence of local minima, but also that some may be even close to the absolute minimum. In some situation the number of local minima may be even over ten.

The use of nonlinear constrains and more importantly the boundary constrains, when well-defined, help reducing the chance to fall on a local minimum instead of the absolute one.

3.6 Attitude Correction Rotation

From the solution to the problem it is possible to determine the direction of maximum power generation during the cometary day, defined as the azimuth $\bar{\alpha}$ in lander's body reference system at which the wall 3 must be pointed at. It is then required to compute the azimuth rotation α_R needed to redirect the wall 3 of the lander towards it (see fig. 2.1).

The possible events are four:

- **Cometary day** The time history of the angles shows that the Sun rises and sets. In this situation the Sun culmination, defined by the maximum value achieved by beta, determines the maximum power direction $\bar{\alpha}$ (chapter 2.1), as the azimuth coupled to $\bar{\beta} = \max(\beta)$.

- **Hovering** This phenomenon happens when the Sun is visible during all the comet revolution, without disappearing under the horizon. Here the interest is to maintain the Sun direction normal to the walls as much as possible. This happens when the wall 3 is directly pointed to the azimuth $\bar{\alpha}$ coupled to angle of minimum elevation $\bar{\beta} = \min(\beta)$.

- **Zenith transit** In this situation the Sun intersects the lander zenith. In this scenario the direction of maximum power production is defined by the azimuth $\bar{\alpha}$ placed midway from the azimuth relative to sunrise α_{Rise} to the one related to sunset α_{Set}, along the arc covered by the Sun during the cometary day.

- **Perpetual night** If the Sun never rises over the horizon the lander remains always in the dark. In this situation the rotation is indifferent as no power production is taking place at all.

Once the beta of maximum power generation is found the relative alpha $\bar{\alpha}$ is recovered: that angle define the direction at which the wall 3 must be pointed at.

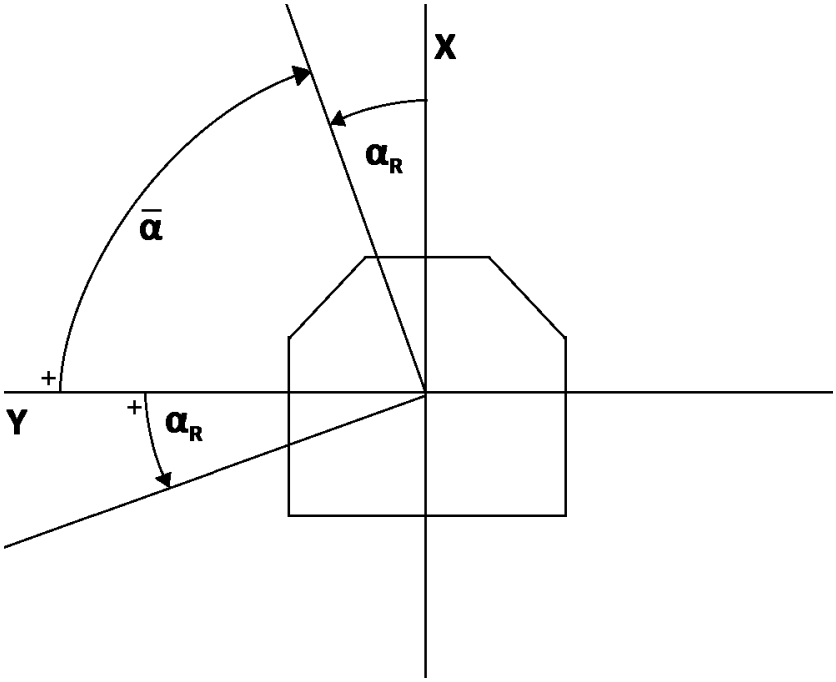

Figure 3.15: Attitude rotation and Sun incidence angle

While the sun incidence angle α is defined positive clockwise around z axis in body reference system, the attitude correction rotation α_R is defined positive counter clockwise, and both start from the y axis. An example is shown in fig. 3.15.

To achieve the smallest rotation it is defined the following algorithm:

$$\alpha_R = \begin{cases} 90 - \bar{\alpha} & 0 \leq -\bar{\alpha} \leq 270^\circ \\ 360 - (\bar{\alpha} - 90) & 270 < \bar{\alpha} < 360 \end{cases}$$

In this way the asset rotation required is always less than 180°.

3.7 GUI: Graphical User Interface

To simplify interaction with the algorithm it has been created a GUI (graphical user interface), capable to load the desired telemetry file, show the telemetry output, and all the main steps of the process through plots display.

In fig. 3.16 it is possible to see the interface: once loaded the telemetry through the relative button, it will be presented the static text “busy”until the solution is computed, then in the plot windows will be shown the MPPT current outputs and the Sun Incidence Angles. Two panels distinguish be-

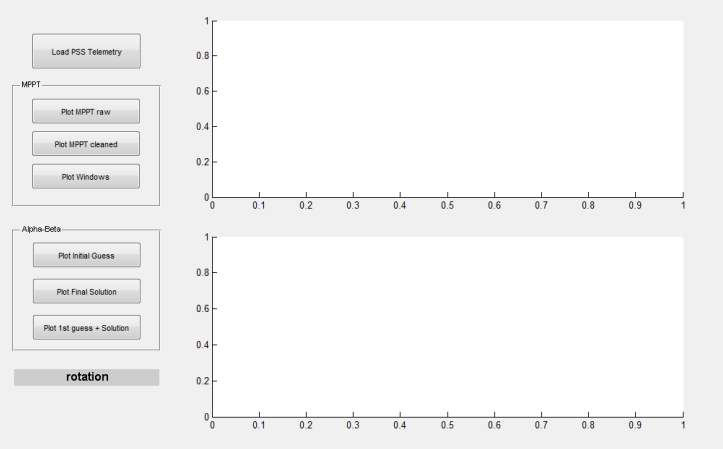

Figure 3.16: Graphical User Interface

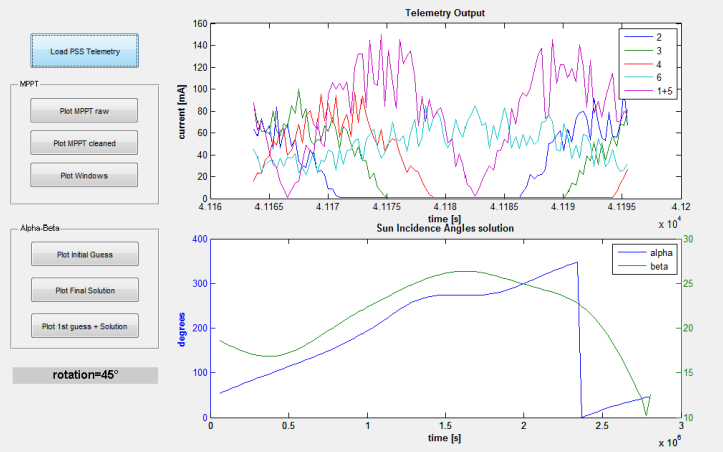

Figure 3.17: Graphical User Interface - solution display

tween MPPT outputs and Sun incidence angles: in the first group it is possible to display between telemetry data, signal cleaned from spurious behaviors and power production windows; in the second between final solution, starting guess and the combinations of the two together with boundary constrains and maximum power direction angles. The rotation required to optimize power production is displayed in the text box. In the GUI are available also the “zoom in”, “zoom out”, “pan”, “data cursor”and “legend ”to navigate through plots display and to extrapolate values. In fig. 3.17 it is possible to see how the solution is presented.

It is also created a text file named as the telemetry file with the values of the Sun incidence angles obtained as solution to the problem.

Chapter 4

Results

In this chapter there will be discussed the results obtained in the most relevant scenarios studied when obtaining Sun incidence angles starting from the power telemetry. The algorithm is tested by using the MPPT simulator presented in chapter 3.1 along with a telemetry simulation provided by DLR.

Regarding the results obtained from the telemetry files obtained from the MPPT simulator, where an exact solutions is held, it will also presented the error regarding $\bar{\alpha}$ maximum power direction angle and relative energy loss.

4.1 Solutions from MPPT simulator

As the angles histories obtained from [11] cover almost all the possible cometary scenarios, it is possible to see how the algorithm, and relative program, solve each single case.

As already presented earlier in this thesis, the possible scenarios the lander may face are four:

- **Cometary day** Presence of night, the Sun rises and set during every cometary revolution. The beta angle presents positive values during while Sun visibility, negative when the lander enters in the dark side of the comet. Eventual α jumps could not be seen if relative beta angle is negative. In fig. 4.1 is present a day-night cycle but it is not present an alpha jump, which instead occurs in fig. 4.2.

- **Hovering** The Sun remains visible during the whole cometary revolution, absence of night. Beta angle remain always positive, alpha changes phase once per revolution. A representative example is shown in fig. 4.3.

- **Zenith transit** In this situation the Sun intersects the Philae zenith direction. As the star transits over the lander, beta reaches maximum value ($\pi/2$) and alpha jump of π. An example is in fig. 4.4.
- **Perpetual night** The lander never sees the Sun, as it never rises over the horizon. It is possible to see a relative beta time history in fig. 4.5.

Each of these scenarios produced a telemetry file through the MPPT simulator: these will be separately studied and the relative Sun incidence angles, obtained through optimization, will be analyzed and compared with the exact solution.

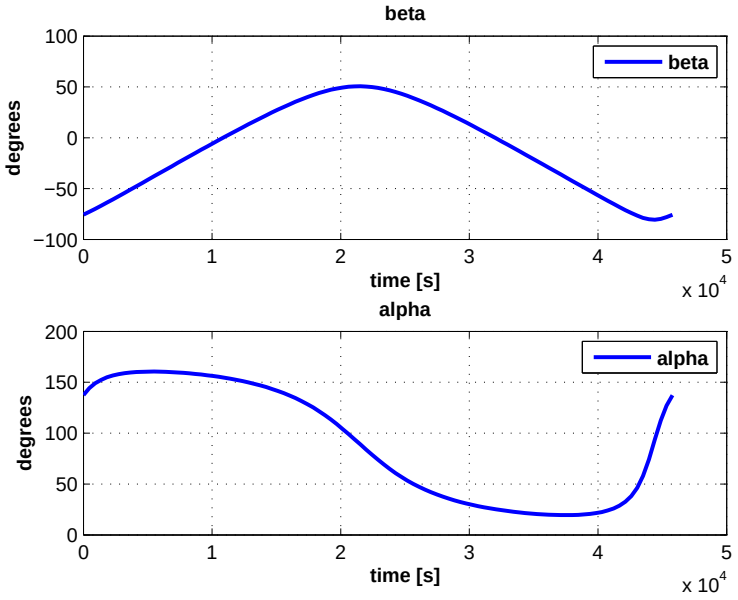

Figure 4.1: Cometary day without α phase change

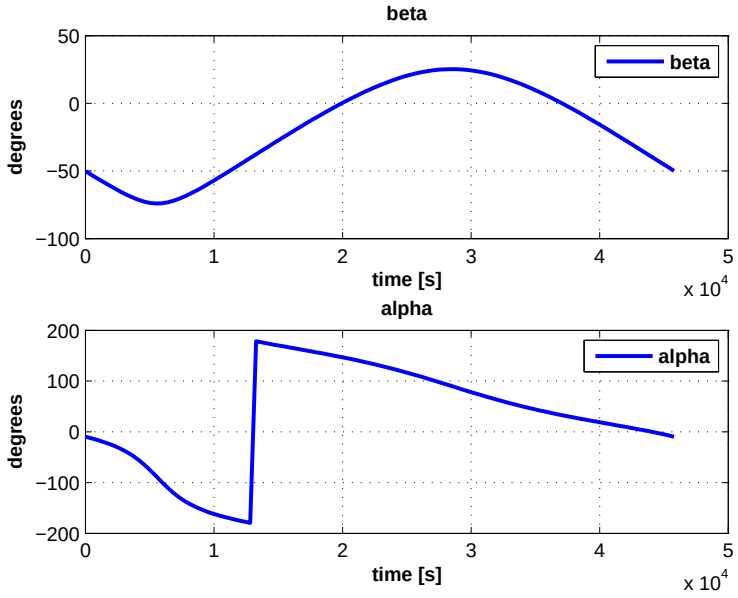

Figure 4.2: Cometary day with α phase change

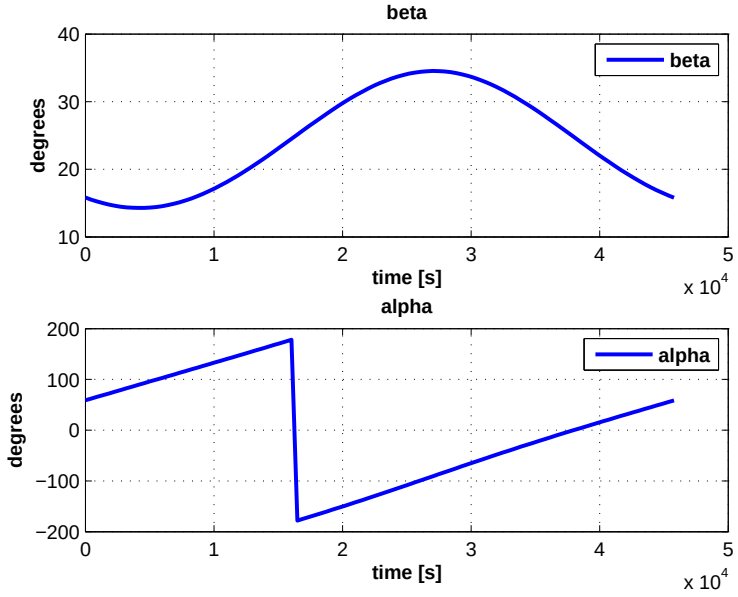

Figure 4.3: Hovering during cometary revolution

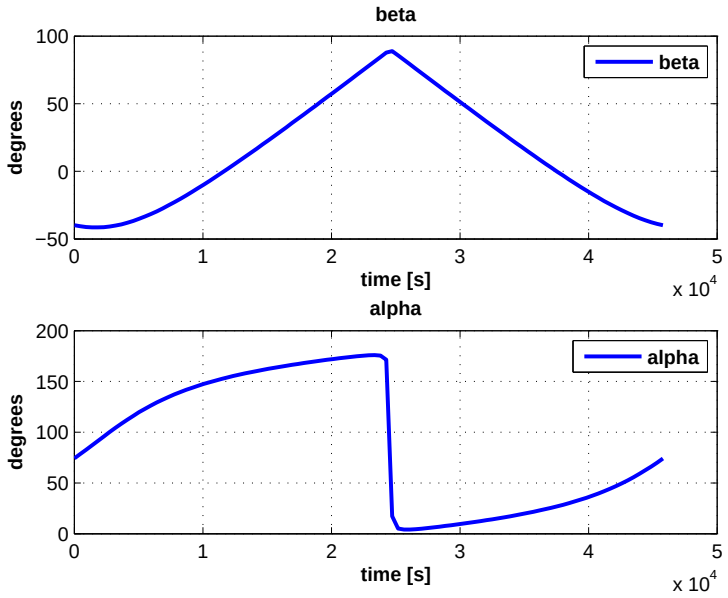

Figure 4.4: Zenith crossing as β reaches maximum

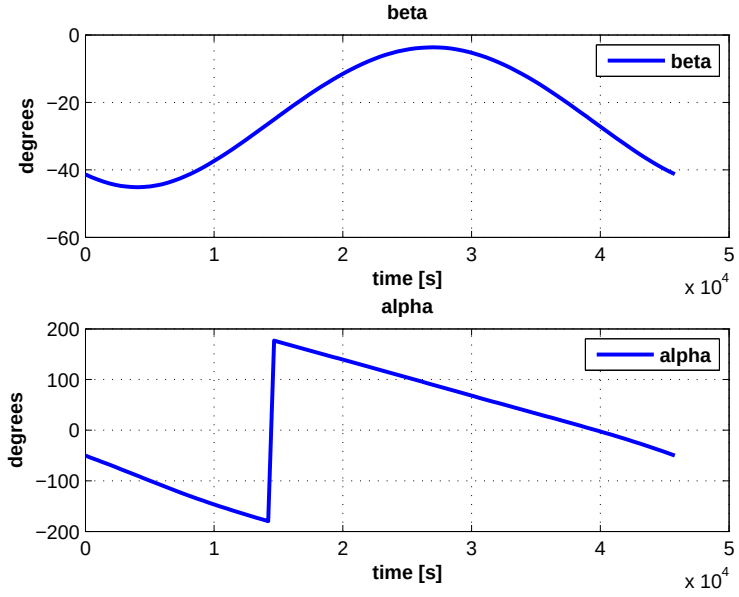

Figure 4.5: Perpetual night on comet

4.1.1 Cometary day solution analysis

The telemetry regarding the cometary day scenario presents the MPPTs current profile shown in fig. 4.6.

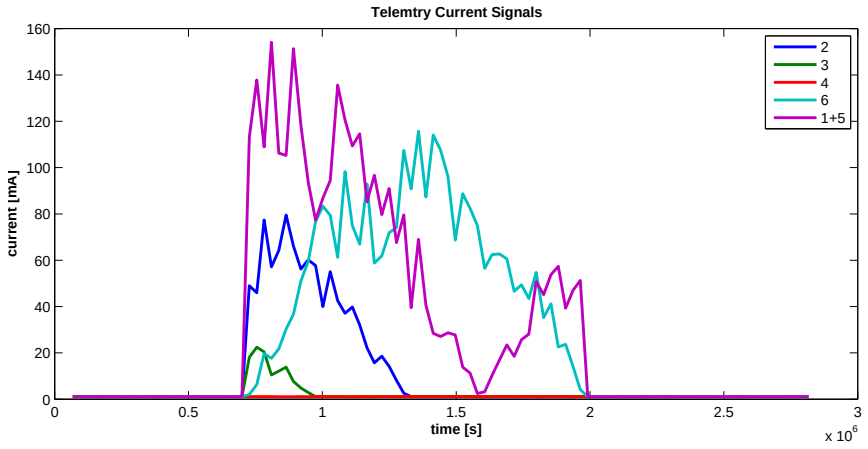

Figure 4.6: Cometary day: telemetry current data

The relative cleaned signals are displayed with the power windows in fig. 4.7. From here it is possible to see the lack of significant power production outside of a specific time period, giving immediately the idea of a day-night cycle.

The Sun incidence angles provided by the algorithm are shown in fig. 4.8. At the beginning the Sun is not visible, and the solution is not computed, leaving a null value. On the contrary when the Sun rises β increases, as it goes up over the horizon, and follows its trajectory until it sets. The α time history instead shows the direction of the sun with respect to the lander. It is possible to see that the Sun incidence angles time histories depict a common cometary day, and the β angle related to optimum power production is the one that present the maximum value during the day. The coupled α angle presents a value of 279.5 degrees, resulting in attitude correction rotation of 170.5 degrees, computed thanks to the algorithm shown in chapter 3.6.

A round up of the solutions computed in the algorithm are showed inside fig. 4.9 together with the exact solution used to simulate the MPPT behavior. It is possible to see how the computed solution shows a good agreement with the exact one, with two main differences: the numerical solution for β presents a trend always lower than the exact one, but given the good accordance the maximum value is reached at the same time; the computed α solution is not exactly the same as the exact solution, and this will lead to a lack in the rotation correction value, but it is still capable to show in a

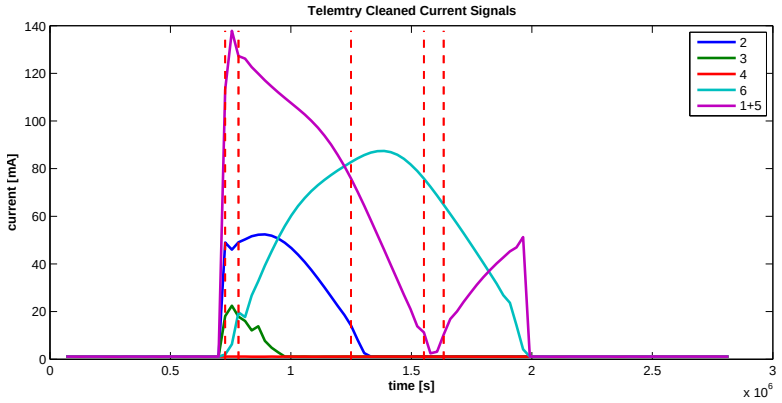

Figure 4.7: Cometary day: cleaned current signals with power production windows

good way the trend of the original angle.

In tab. 4.1 it is possible to see the difference between exact and computed solutions: the error is not irrelevant, but if we look at tab. 4.2 we can see that the total gain is more than significant, with an increment of almost 60%. All these values are computed by using the maximum power point on the IV curves, since the MPPT random effect loss would effect the results and ruin a useful comparison.

Lastly in fig. 4.10 are showed all the exact, computed and original Sun incidence angles histories.

Table 4.1: Cometary day: Values and Errors

	Exact	Computed	Error
α correction [°]	141.8	170.5	28.8
Power Production [Wh]	82.77	78.21	-4.56

Table 4.2: Cometary day: Energy gain

	Old	New	Total gain
Power Production [Wh]	49.1	78.2	29.1

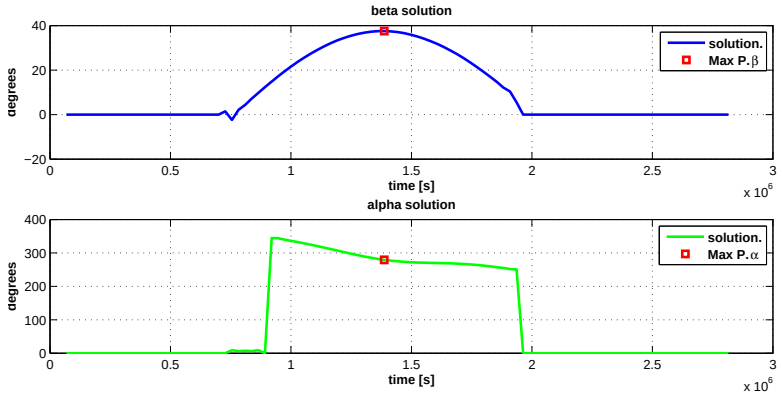

Figure 4.8: Cometary day: β and α solution

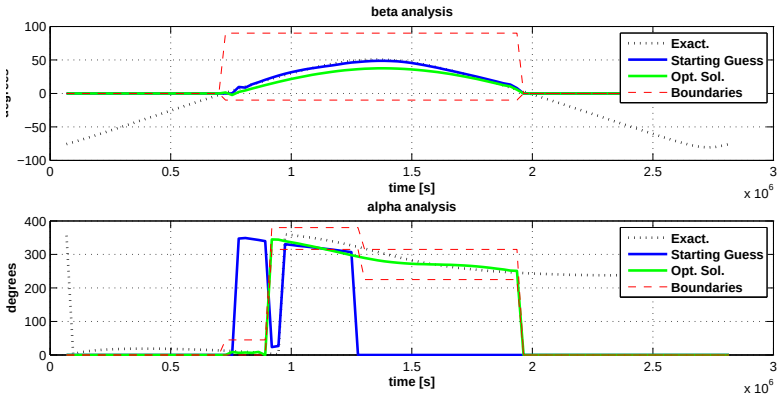

Figure 4.9: Cometary day: exact and computed solutions

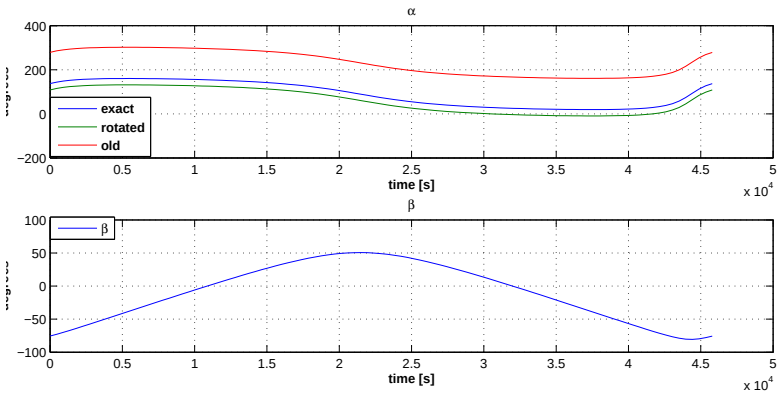

Figure 4.10: Cometary day: α histories

4.1.2 Hovering solution analysis

A telemetry recalling a hovering scenario is shown in fig. 4.11: during all the time there is at least on side wall (1 to 5) producing power, meaning there is always Sun visibility.

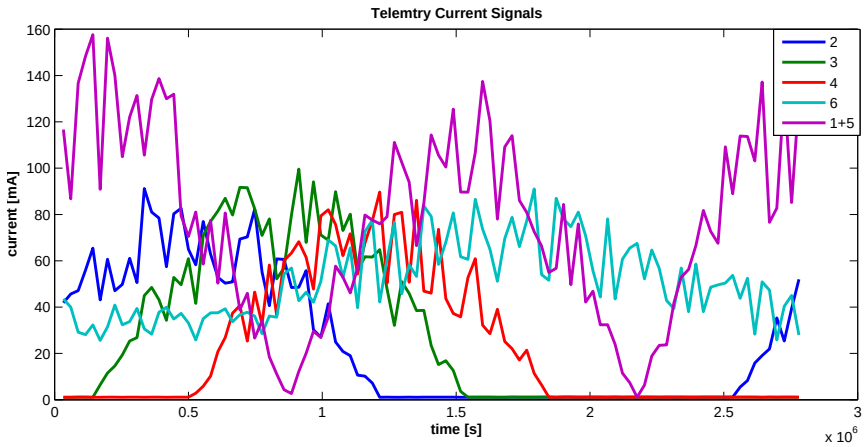

Figure 4.11: Hovering: telemetry current data

The relative cleaned signals are displayed with the power windows in fig. 4.12. It is clearer that there is hovering: wall 6 never stops producing power output, meaning the Sun is always over the horizon. Also it is already possible to have an idea of where the Sun is located during the cometary day: when MPPT5_1 has no current output, the Sun is directly facing wall3 when the relative MPPT has maximum output, or the back wall of the lander when no side panels are producing power.

The Sun incidence angles provided by the algorithm are shown in fig. 4.13. The β time history once more show that there is hovering, as the elevation angle is always more than null value. During hovering the optimum attitude, so to obtain maximum power production, is where wall3 is directly pointed at the direction marked by minimum β reached during cometary revolution. The algorithm shows a solution of beta value clearly erroneous: this is due to the fact that at the limits of the solutions the misbehaviors are more pronounced. The sinusoid trend of the β angle helps to find the correct rotation:the valley represents a good place to look for the minimum. This shows clearly that the main task of the algorithm is to find the trend of the Sun incidence angles: a critical study of the results is required to obtain the attitude rotation needed.

Once taken as maximum power production angles $\beta = 16.7°$ and $\alpha = 24.8°$, the attitude rotation is computed, and in tab. 4.3 it is possible to

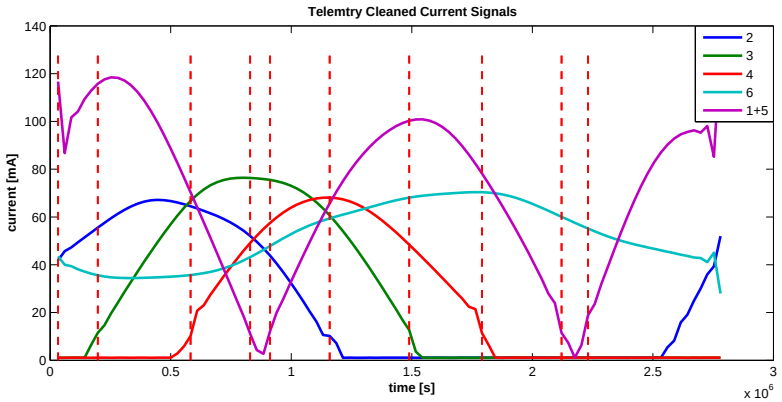

Figure 4.12: Hovering: cleaned current signals with power production windows

see the difference between exact and computed solutions, where the relative error is low. The algorithm may fail when choosing the Sun incidence angles related the maximum power production, but the computed trends of the angles give the chance to manually select the correct values. In tab. 4.4 we can see that the gain in terms of energy produced is not high, as the hovering by itself is an optimal scenario regarding this aspect, but the Watts obtained by attitude correction still do the difference.

In fig. 4.14 are shown the exact and computed solutions: it is possible to appreciate how the algorithm computed angle trends really close to the exact ones. Lastly in fig. 4.15 are showed all the exact, computed and original Sun incidence angles histories.

Table 4.3: Hovering: Values and Errors

	Exact	Computed	Error
α correction [°]	72.65	65.18	-7.47
Power Production [Wh]	83.7	83.7	-0.02

Table 4.4: Hovering: Energy gain

	Old	New	Total gain
Power Production [Wh]	81.5	83.7	2.2

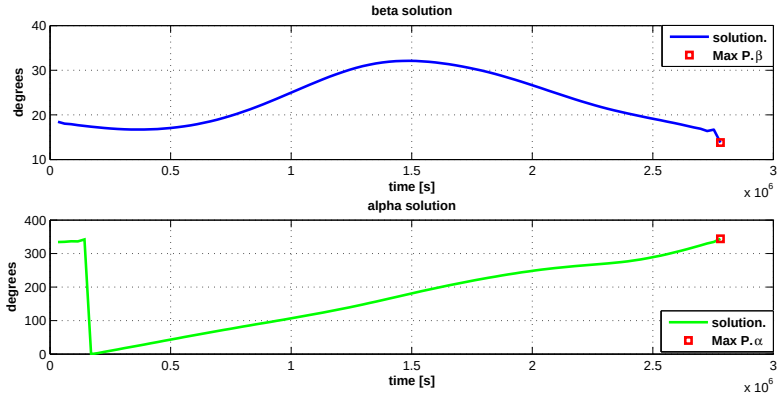

Figure 4.13: Hovering: β and α solution

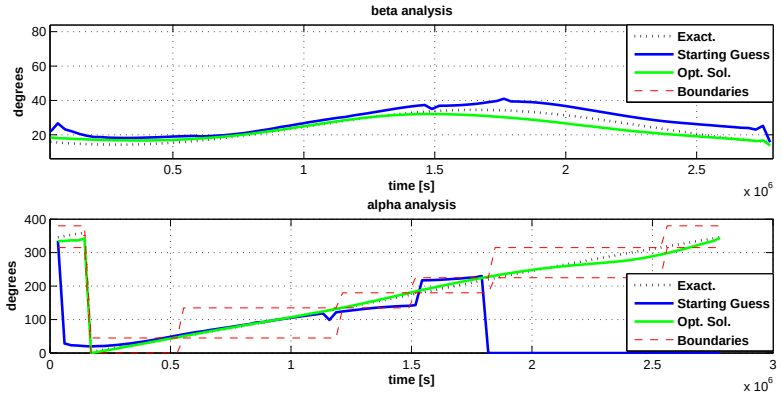

Figure 4.14: Hovering: exact and computed solutions

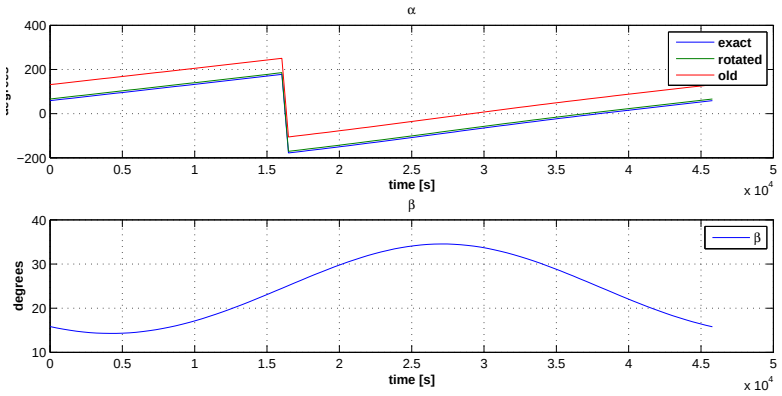

Figure 4.15: Hovering: α histories

4.1.3 Zenith crossing solution analysis

A scenario of zenith transition is recognizable in two ways: by analyzing the telemetry signals and by looking at the change of phase in the α boundary constrains. In fig. 4.16: it is possible to see that MPPT 6 reaches maximum power production exactly when all the others stop: a similar situation happens when during a common cometary day the Sun reaches maximum elevation exactly at $\alpha = 270°$, but this is not the case as more than one side panel stop simultaneously, meaning that the Sun is transiting over the lander instead of around.

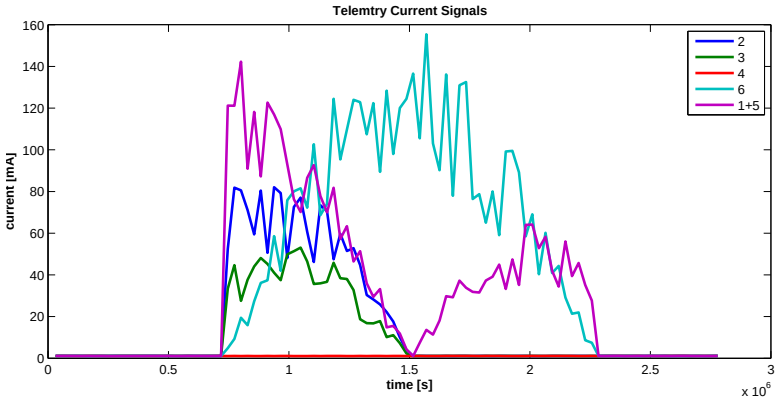

Figure 4.16: Zenith transit: telemetry current data

The relative cleaned signals are displayed with the power windows in fig. 4.17: here it is more clearly showed what exposed in the previous paragraph.

The Sun incidence angles provided by the algorithm are shown in fig. 4.18. The change of phase in the α solution is new hint of zenith transition: this could be due to restart of the azimuth angle, but this is not possible as that would requires MPPT5_1 to produce a current output, which is not. Between all scenarios this one is the hardest in obtaining a clear solution, as all the misbehaviors are exasperated when the incidence of the light on the panels is low, which thing happens in a really small time period on almost every lander side wall during zenith transition.

The Sun describes a trajectory whose top overlaps with lander's zenith, while sunrise and sunset azimuths α_{Rise} and α_{Set} divide the horizon in two arcs: one, smaller, that covers the Sun movement direction during cometary day; one, bigger, that refers to the deep space of the hemisphere surrounding the lander. The azimuth of maximum power direction $\bar{\alpha}$ is the angle placed midway between α_{Rise} and α_{Set} inside the azimuths arc regarding Sun

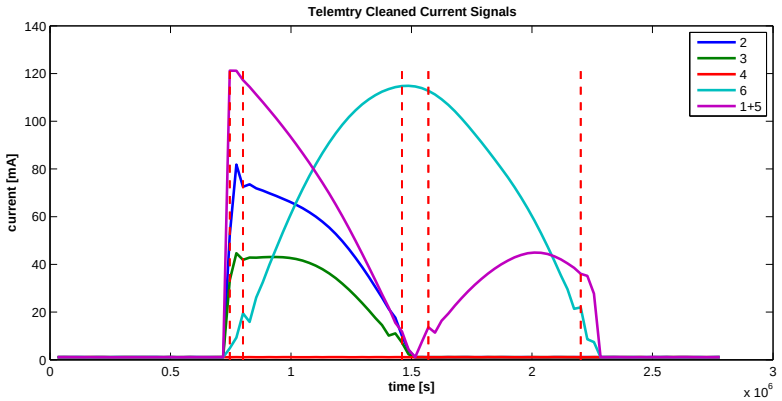

Figure 4.17: Zenith transit: cleaned current signals with power production windows

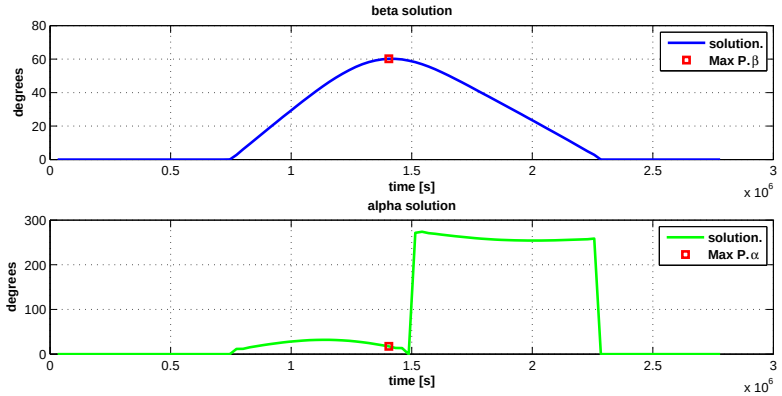

Figure 4.18: Zenith transit: β and α solution

trajectory.

Sunrise and sunset azimuths must then be recovered, but the final solution presented in fig. 4.18 is not clear enough to extrapolate such values. To obtain the informations needed, it is necessary to look at fig. 4.20. Here we can see that on one side the starting guess has a better behavior while on the other one the final solution seems correct enough. By critically analyzing the results, with the help of the boundaries constrains, the following values are extrapolated: $\alpha_{Rise} = 40°$ and $\alpha_{Set} = 260°$. The azimuth arc to look for is the smaller one.

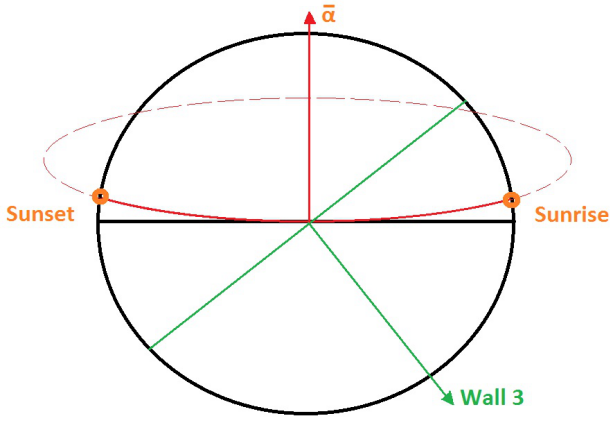

Figure 4.19: Zenith transit: maximum power production $\bar{\alpha}$

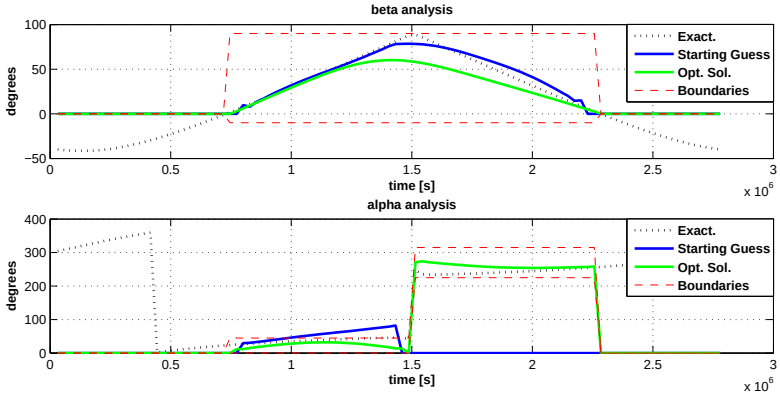

Figure 4.20: Zenith transit: exact and computed solutions

In fig. 4.19 it is possible to see the situation the lander is facing. The attitude rotation processed by the algorithm is not correct, as it is required a critical analysis it is not capable to process, therefore here $\bar{\alpha}$ is computed as in 4.1, giving a rotation $\alpha_R = 130°$ obtained as in chapter 3.6.

$$\bar{\alpha} = \frac{|\alpha_{Rise} - \alpha_{Set}|}{2} + \alpha_{Set} = \frac{|40 - 260|}{2} + 260 = \frac{400 - 260}{2} + 260 = 330 \quad (4.1)$$

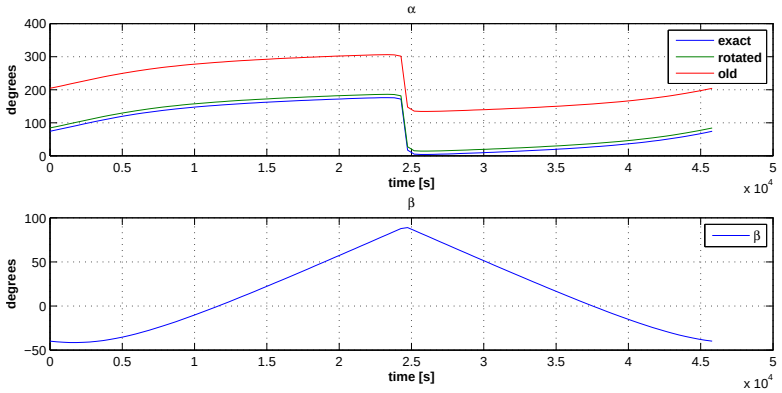

Figure 4.21: Zenith transit: α histories

We can see in fig. 4.20 that the final solution is not well representing the exact trend of the Sun incidence angles. As told before the zenith transit scenario stresses the misbehaviors of the current signals, but being easily recognizable it ensures anyway the chance to identify the direction $\bar{\alpha}$.

Table 4.5: Zenith transit: Values and Errors

	Exact	Computed	Error
α correction [°]	130.0	120	-10.0
Power Production [Wh]	88.7	88.1	-0.6

Table 4.6: Zenith transit: Energy gain

	Old	New	Total gain
Power Production [mW]	57.3	88.1	30.8

In fact in tab. 4.5 it is possible to see that the attitude rotation computed by graphic analysis is capable to point the lander close enough to maximum power production direction: this ensure a significant energy gain during the cometary day, as seen in tab. 4.6. Lastly in fig. 4.21 are showed all the exact, computed and original Sun incidence angles histories.

4.2 Solutions from DLR telemetries

During the development of the algorithm two telemetries were provided: one from an actual check test during mission flight (PST), seen in chapter 2.3, useful to see how a telemetry file is configured and the possible disturbes arising from MPPT scanning; one from a hardware simulation (GRM simulation) specifically done to test the thesis algorithm.

For these telemetries no exact solution has been provided, and in the following paragraphs are showed and discussed the results obtained.

Power system test telemetry Here will presented the results obtained from such telemetry, but no reliability must be given as the current signals where sampled in an environment that does not respect the assumptions taken in chapter 3.1. In fact the Rosetta orbiter, at which Philae is attached to, has prominences and reflective surfaces that deeply affect the SAs working conditions.

In fig. 4.22 are showed the MPPT current outputs, and in fig. 4.23 the corresponding cleaned signals together with the power production windows.

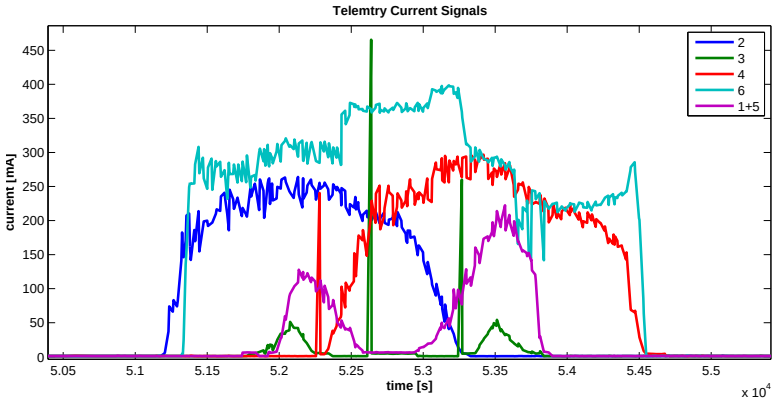

Figure 4.22: Flight telemetry: telemetry current data

The solution for the Sun incidence angles is presented in fig. 4.24, while relative boundary constrains and starting guess are showed in fig. 4.25. No attitude rotation is computed since the telemetry is not representing a cometary scenario.

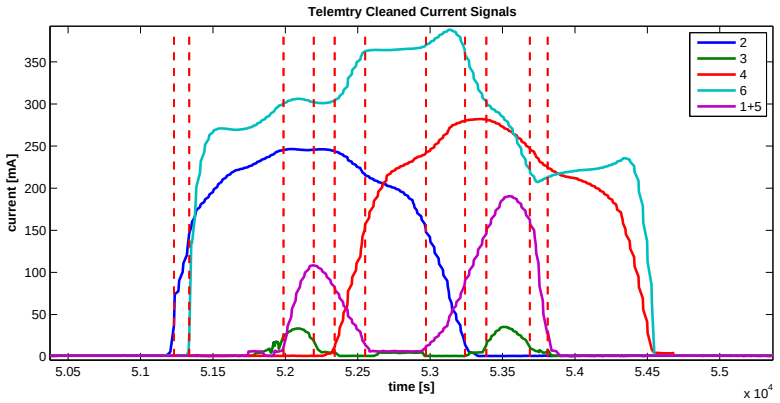

Figure 4.23: Flight telemetry: cleaned current signals with power production windows

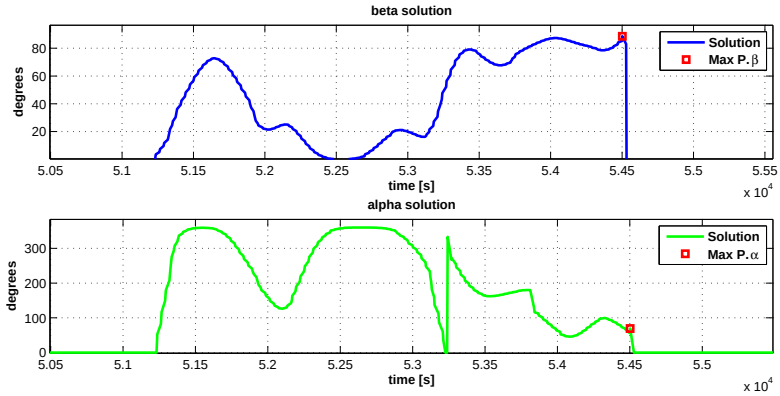

Figure 4.24: Flight telemetry: β and α solution

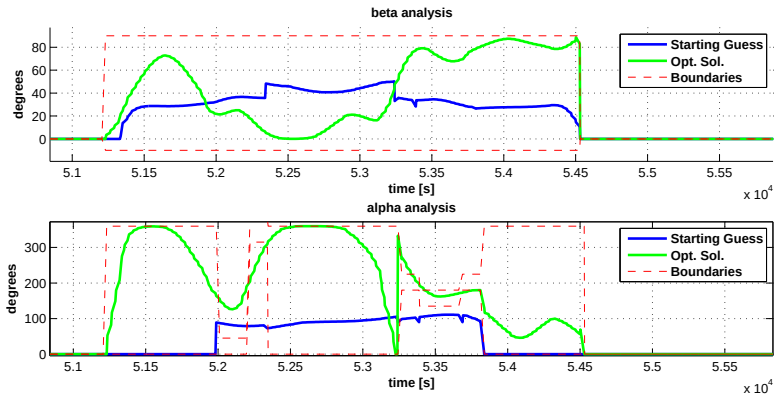

Figure 4.25: Flight telemetry: solution with starting guess

GRM simulation This telemetry is obtained through an hardware simulator, and it serves as test telemetry for the algorithm. The MPPT raw outputs are showed in fig. 4.26 and the corresponding clean signals in fig. 4.27 together with power production windows.

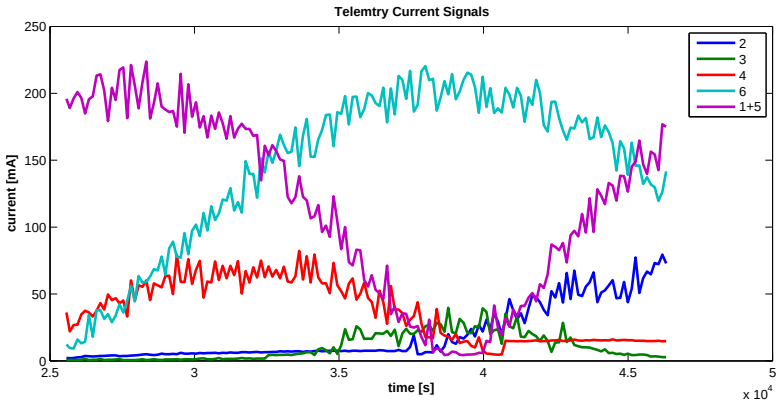

Figure 4.26: Simulation telemetry: telemetry current data

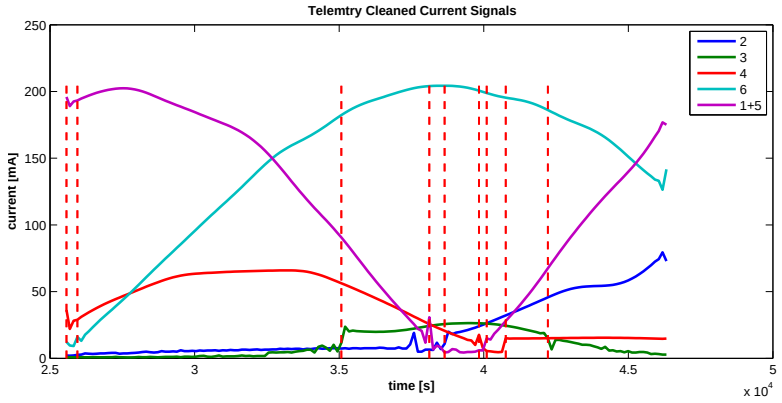

Figure 4.27: Simulation telemetry: cleaned current signals with power production windows

It is immediately noticeable how the telemetry is not covering a whole cometary day. By analyzing the signals we can see that MPPT6 maximum output is reached when MPPT5_1 is not producing power, while MPPT3 reaches its top current output, even if not comparable with respect to the others MPPTs. By adding the fact that MPPT4 and MPPT5_1 have maximum power production at the beginning of the day, while MPPT6 signal is low, and MPPT2 with MPPT5_1 towards the end, it is possible to have already an hint of how the Sun is located throughout the day.

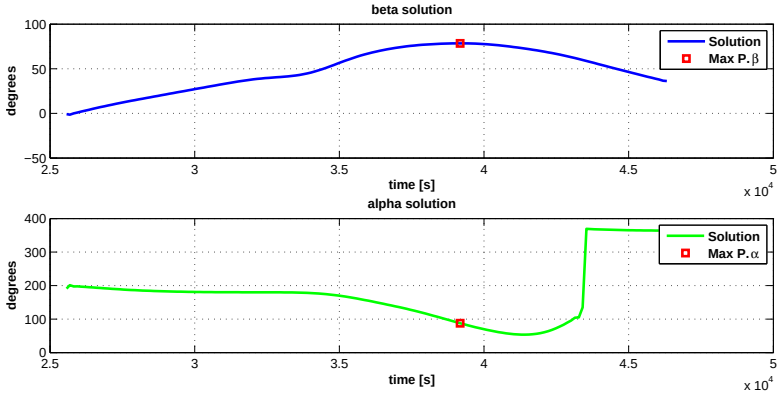

Figure 4.28: Simulation telemetry: β and α solution

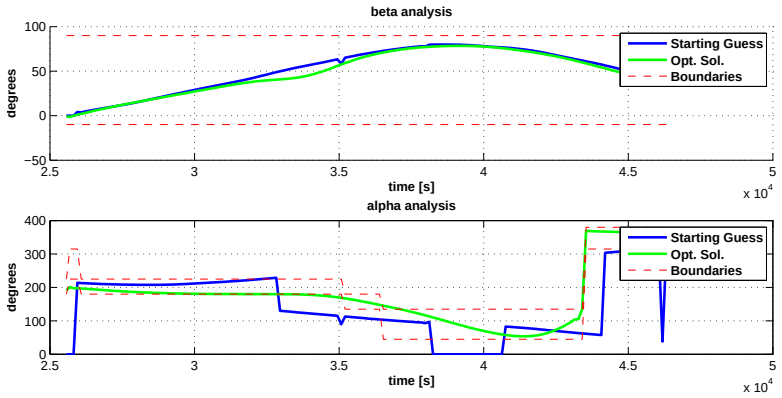

Figure 4.29: Simulation telemetry: solution with starting guess

The computed solution is showed in fig. 4.28. The algorithm chooses as maximum power direction the one of minimum β, as it is always positive in the time period: but as only around 6 hours are sampled, it is foreseeable the presence of night. It is then required to force the algorithm to look for maximum elevation as in a common cometary day.

The values obtained are $\bar{\beta} = 78.5°$ and $\bar{\alpha} = 87.7°$, resulting in a attitude rotation of $\alpha_R = 2.3°$. By looking to the MPPT cleaned signals and to the α solution trend it is clear that the lander is already really close to optimum orientation with respect to Sun trajectory during cometary day. The α change of phase is due to ending and starting over the cycle in lander body reference system. The starting guess and boundary constrains are presented along with the final solution in fig. 4.29.

Chapter 5

Conclusions

Under the assumptions presented in chapter 3.1, starting from a power telemetry file arranged as in chapter 2.3, the algorithm presented in the body of this thesis proved to be able to satisfy the request of reconstructing the time histories of Sun incidence angles, defined as α, azimuth, and β, elevation, in lander Philae's body reference system.

Other than recognition of the event of perpetual night, where no power production takes place, the results in chapter 4 show that, starting from the lander MPPTs current signals sampled during the cometary day, the algorithm is capable to determine the direction of the Sun inside the time period defined in the telemetry file. While great accuracy is achieved during common cometary day or Hovering, whose represent the most plausible working conditions, some mismatches from the exact solution arise when facing zenith transition: this situation is a borderline case, and the chances of this happening are few, but it still represents a possible scenario.

To solve eventual problems the algorithm provides to the user a series of informations other than final solution, such as, for example, starting guess, boundary constrains and cleaned current signals with power production windows: thanks to these added details through critical analysis it is recovered the more likely scenario the lander is facing.

Regarding the attitude correction rotation, the algorithm provides the azimuth and the elevation relative to the direction of optimum power production, and the corresponding α_R to point the lander's wall 3 towards it. The results must not be taken blindly, but through critical analysis the user must validate them: in case they are not satisfying all the added informations must be used to recover the exact values. An example on how properly the algorithm works is shown in the results regarding the hardware simulation, were the results obtained are considered clearly satisfying even without an exact solution to compare to.

In conclusion the algorithm proves to provide the instruments and the informations needed to recover the Sun incidence angles and the relative rotation to maximize power production during Long Term Science operative phase on comet 67P-Churyumov-Gerasimenko.

Nomenclature

Acronyms

AU Astronomical Unit

CNES Centre National d'Etudes Spatial

D-SAS Diode Solar Array Simulator

DLR Deutches zentrum fur Luft und Raumfahrt

ESOC European Spacecraft Operations center

ESS Electric Support System

FL-SAS Fast Loop Solar Array Simulator

FSS First Science Sequence

GRM Ground Reference Module

GUI Graphical User Interface

HW HardWare

LB Lower Bound

LCC Lander Control Center

LILT Low-Intensity Low-Temperature

LTS Long Term Science

MPP Maximum Power Point

MPPT multiple power point tracker

PSAS Philae Solar Array Simulator

PSS Power SubSystem

SA Solar Array

SAS Solar Array System

SC Solar Constant

SD2 Sampler Drill and Distribution system

SDL Separation, Descending and Landing

SONC Science operative and Navigation Center

SW SoftWare

UB Upper Bound

Greek symbols

α Sun incidence azimuth

α_R attitude rotation

α_{Rise} Sunrise azimuth

α_{Set} Sunset azimuth

β Sun incidence elevation

η Total Efficiency

ϑ panel incidence angle

Roman symbols

$\mathbf{x}_0$ Parameters starting guess

A Soalr Array area

F Performance index

g Non linear constrain function

I_{SC} Short Circuit currnt

m Smooth width

n_c Number of combinations of 2 panels lit

n	Solar array panel normal versor
P	Power output
p	Parameters of the system
S	Sun direction vector
s	Sun direction versor
s	White noise standard deviation
t	Time
u	Vector of algebraic variables
V_{OC}	Open Circuit voltage
x	vector of the parameters
$\bar{Y}$	Interpolated computed current output
$\hat{Y}$	Telemetry current output
Y	Computed current output

Bibliography

[1] "DLR Rosetta Mission Brochure - Journey to a comet", Deutsches Zentrum for Luft und Raumfahrt, 2008

[2] "Hubble Space Telescope observations of the nucleus and inner coma of comet 67P/Churyumov-Gerasimenko ", VV.AA., Astronomy & Astrophysics 458, 2006

[3] "Rosetta space mission The solar array photovoltaic assembly ", M. Psco, A. Ercoli Finzi, XIX Congresso Nazionale AIDAA, September 2007, Forlì (FC)

[4] VV.AA., "The Rosetta Mission: flying towards the origin of the solar system", - Technische Universitat Braunschweig, 2006

[5] VV.AA., "Rosetta Lander - System Status after Five Years in Space", Aerotecnica Vol.88, No.4, 2009

[6] S. Ulamec, J. Biele, "From the Rosetta Lander Philae to an Asteroid Hopper: lander concepts for small bodies missions", German Aerospace Center (DLR), 2004

[7] F. Topputo, F. Bernelli-Zazzera, A. Ercoli-Finzi, "On-Comet Power Production: the Case of Rosetta Lander Philae", Proceedings of the European Planetary Science Congress 2010, Vol. 5, EPSC2010-96, Rome, September 2010

[8] F. Topputo, F. Bernelli-Zazzera, F. Ercoli-Finzi, "Solar Array Simulators for Low Power Space Missions", Proceedings of the 3rd CEAS Air & Space Conference, 2011, 978-88-96427-18-7

[9] F. Topputo, A. Ercoli-Finzi, F. Bernelli-Zazzera, "LTS Phase: The Power Production Standpoint", Venice, 2009

[10] Jhon T. Betts, "Practical Methods for Optimal Control and Estimation Using Nonlinear Programming - 2nd ed.", Siam, 2010

[11] G. Pinzan, “Landing site selection for Rosetta lander Philae though a multidisciplinary approach”, MS Thesis, Politecnico of Milano, 2012

[12] “PHILAE Solar generator models ”, Jens Biele, 2005, RO-LAN-TN-3013-JBI